nature biotechnology

ARTICLES

https://doi.org/10.1038/s41587-022-01377-0

Frequent aneuploidy in primary human T cells after CRISPR–Cas9 cleavage

Alessio David Nahmad[1,2,9], Eli Reuveni[3,9], Ella Goldschmidt[4,9], Tamar Tenne[5], Meytal Liberman[5], Miriam Horovitz-Fried[1,2], Rami Khosravi[6], Hila Kobo[7], Eyal Reinstein[5,8], Asaf Madi[4,10] ✉, Uri Ben-David[3,10] ✉ and Adi Barzel[1,2,10] ✉

Multiple clinical trials of allogeneic T cell therapy use site-specific nucleases to disrupt T cell receptor (TCR) and other genes[1–6]. In this study, using single-cell RNA sequencing, we investigated genome editing outcomes in primary human T cells transfected with CRISPR–Cas9 and guide RNAs targeting genes for TCR chains and programmed cell death protein 1. Four days after transfection, we found a loss of chromosome 14, harboring the TCRα locus, in up to 9% of the cells and a chromosome 14 gain in up to 1.4% of the cells. Chromosome 7, harboring the TCRβ locus, was truncated in 9.9% of the cells. Aberrations were validated using fluorescence in situ hybridization and digital droplet PCR. Aneuploidy was associated with reduced proliferation, induced p53 activation and cell death. However, at 11 days after transfection, 0.9% of T cells still had a chromosome 14 loss. Aneuploidy and chromosomal truncations are, thus, frequent outcomes of CRISPR–Cas9 cleavage that should be monitored and minimized in clinical protocols.

The effect of engineered T cells in the clinic continues to grow. Five treatments using chimeric antigen receptor (CAR) T cells have received regulatory approval in different B cell malignancies[7]. Hundreds of ongoing clinical trials, for multiple additional indications, are applying different variations of CARs or engineered TCRs in an attempt to improve efficacy, safety and scalability[1]. Importantly, the approved CAR T therapies all entail the cumbersome, expensive and time-consuming manipulation of autologous T cells. Many current efforts are, therefore, directed at facilitating the engineering and banking of allogeneic CAR/TCR T cell products. In this approach, the endogenous TCR of engineered allogeneic T cells has to be disrupted to prevent graft versus host disease, and this is most often achieved using site-specific nucleases such as meganucleases[2], TALENs[3,4], megaTALs and CRISPR–Cas9 (ref. [5]). Cleaving the TCR loci can further serve for the directed integration of CAR and engineered TCR genes, allowing uniform expression, enhancing T cell potency and delaying exhaustion[8–11]. Finally, additional genes, beyond the TCR chains, may be disrupted to improve T cell function[12], confer drug resistance[13] or avoid checkpoint inhibition[14].

Site-specific nucleases can be highly potent[15], but they are associated with a variety of undesired outcomes. Cas9 can be immunogenic in vivo, eliciting both humoral and cellular responses[16]. We recently demonstrated that Cas9 activates the p53 pathway and selects for p53-inactivating mutations[17]. Off-target cleavage can, in turn, be reduced but not eliminated[18], and small on-target insertions and deletions are common, even when providing a donor template for gene correction or insertion. Importantly, CRISPR–Cas9 cleavage can also lead to gross chromosomal aberrations. In particular, CRISPR–Cas9 cleavage leads to large deletions in early mouse[19,20] and human embryos[21] as well as in embryonic stem cells and induced pluripotent stem cells[22,23]. Moreover, chromosomal truncations were reported after CRISPR–Cas9 cleavage in mouse and human cell lines[24,25], and entire chromosome loss has resulted from CRISPR–Cas9 cleavage in human embryos[26]. Recently, chromothripsis, defined as multiplicity of gross genomic rearrangements in a one-off cellular crisis, was inferred in mobilized human CD34$^+$ cells after CRISPR–Cas9 cleavage of the BCL11A gene in a clinically relevant setting[27,28], with possible ramifications for the development of gene therapies for hemoglobinopathies. Finally, in the first US clinical trial involving CRISPR–Cas9, Stadtmauer et al.[6] aimed at disrupting the TCR and programmed cell death protein 1 (PDCD1) loci for allogeneic T cell therapy and reported the detection of chromosomal translocations whose frequency decreased over time after infusion into patients.

In this study, we used the same guide RNA sequences as did Stadtmauer et al.[6] to target the TCR and PDCD1 loci in primary human T cells with CRISPR–Cas9. Using a novel unbiased approach, based on single-cell RNA sequencing (scRNA-seq), corroborated by fluorescence in situ hybridization (FISH) and digital droplet PCR (ddPCR) analyses, we detected frequent aneuploidy and truncations of the chromosomes harboring the targeted loci.

Results

scRNA-seq reveals chromosome 14 aneuploidy after CRISPR–Cas9 cleavage. We hypothesized that double-strand DNA breaks, induced by site-specific nucleases, may sometime result in chromosomal truncations and aneuploidy due to failure of DNA repair. We further conjectured that such adverse outcomes could be detected and monitored, in a high-throughput manner, by following

[1]School of Neurobiology, Biochemistry and Biophysics, Faculty of Life Sciences, Tel Aviv University, Tel Aviv, Israel. [2]Varda and Boaz Dotan Center for Advanced Therapies, Tel Aviv Sourasky Medical Center and Tel Aviv University, Tel Aviv, Israel. [3]Department of Human Molecular Genetics & Biochemistry, Faculty of Medicine, Tel Aviv University, Tel Aviv, Israel. [4]Department of Pathology, Faculty of Medicine, Tel Aviv University, Tel Aviv, Israel. [5]Medical Genetics Institute, Meir Medical Center, Kfar-Saba, Israel. [6]Single-Cell Genomics Core, Faculty of Medicine, Tel Aviv University, Tel Aviv, Israel. [7]Genomics Research Unit, Faculty of Life Sciences, Tel Aviv University, Tel Aviv, Israel. [8]Faculty of Medicine, Tel Aviv University, Tel Aviv, Israel. [9]These authors contributed equally: Alessio David Nahmad, Eli Reuveni, Ella Goldschmidt. [10]These authors jointly supervised this work: Asaf Madi, Uri Ben-David, Adi Barzel. ✉e-mail: asafmadi@tauex.tau.ac.il; ubendavid@tauex.tau.ac.il; adibarzel@gmail.com

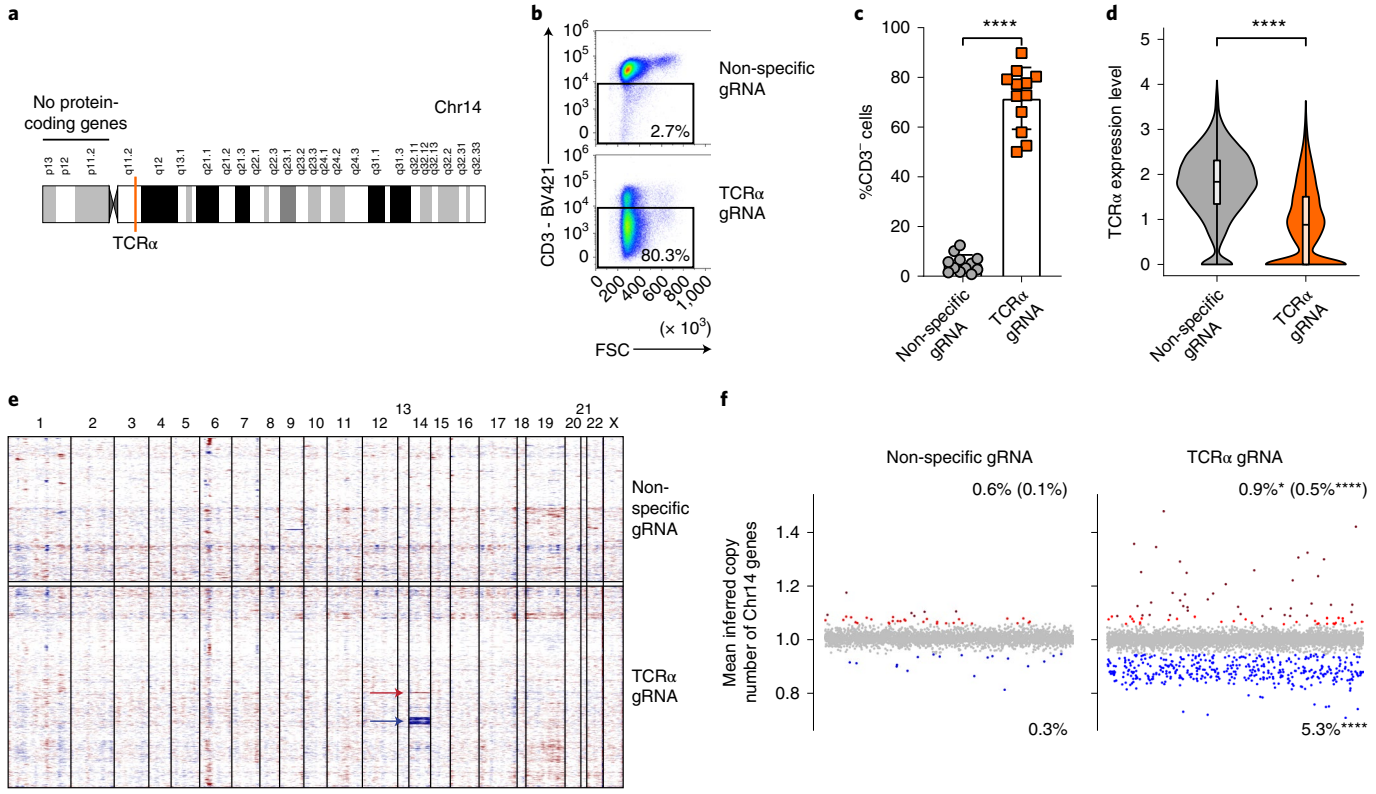

Fig. 1 | Targeting the TCRα locus using CRISPR–Cas9 leads to chromosome 14 aneuploidy. a, Schematic depiction of human chromosome 14 (Chr14). The target locus is indicated in orange. **b**, Flow cytometry example of TCR ablation in primary human T cells 4 days after CRISPR–Cas9 RNP electroporation. Cells were electroporated with Cas9 and either a non-specific gRNA or a TCRα-targeting gRNA. **c**, Quantification of **b**. Each dot represents an independent experiment. Mean value, standard deviation and individual experiments are indicated. $n=12$, $^{****}P<0.0001$, two-sided unpaired Wilcoxon test. **d**, A reduction in TCRα expression is evident in the scRNA-seq. The violin plots correspond to TCRα expression level in cells treated with either a non-specific gRNA or the TCRα-targeting gRNA. Upper and lower boundaries, median and quartiles are indicated. $^{****}P<0.0001$, two-sided unpaired Wilcoxon test. **e**, Heat map depicting gene copy numbers inferred from scRNA-seq analysis after treatment with either non-specific or TCRα-targeting gRNAs. Each line represents an individual cell. The color coding indicates an increase (red) or decrease (blue) in copy number of genes along the chromosomes, ordered in columns. Arrows indicate gain (red) or loss (blue) of chromosome 14. **f**, Each dot represents the mean inferred copy number of genes coded on chromosome 14 in each cell treated with a non-specific gRNA (left) or a TCRα-targeting gRNA (right). Cells are marked with dots spread along the *x* axis. The dots are colored red and blue when corresponding to cells with a chromosome 14 gain or loss, respectively, if their mean inferred gene copy number is >2 standard deviations (blue and red) or 3 standard deviations (dark red) from the population's mean. $n=6{,}055$ and $n=7{,}700$ for non-specific (left) or TCRα-targeting (right) gRNA treated cells, respectively. $^{*}P=0.0148$ and $^{****}P<0.0001$ for Fisher's exact test comparing chromosome 14 gain or loss, respectively, between cells treated with the TCRα gRNA and cells treated with a non-specific gRNA, with a cutoff of 2 standard deviations. $^{****}P<0.0001$, Fisher's exact test comparing chromosome 14 gain between cells treated with the TCRα gRNA and cells treated with a non-specific gRNA, with a cutoff of 3 standard deviations, for which the frequency of cells is indicated in parentheses.

concerted changes in gene expression along chromosomes. To analyze chromosomal truncations and aneuploidy in a clinically relevant setting, we first performed CRISPR–Cas9 ribonucleoprotein (RNP) electroporation into primary human T cells using a single guide RNA (gRNA) targeting the TCRα locus (Fig. 1a). Notably, we used the same gRNA sequence as used clinically in T cells by Stadtmauer et al.[6]. As a control, we used an irrelevant gRNA[15], with no matching target in the human genome. The TCRα locus was successfully targeted in more than 50% of the cells (Fig. 1b,c and Extended Data Fig. 1). Four days after transfection, samples were subjected to scRNA-seq (Methods). The transcriptional downregulation of TCRα was confirmed (Fig. 1d), and the transcriptional landscapes of the cells were used to infer copy number alterations using a well-established method (inferCNV)[29,30]. Strikingly, 5.3% of the cells in the TCRα-targeted sample had expression patterns indicating a chromosome 14 loss (Fig. 1e,f). In addition, among these cells, chromosome 14 was an extreme outlier in the mean number of genes with undetected expression ($P<0.0001$; Extended Data Fig. 1). Notably, a chromosome 14 q-arm truncation at the TCRα locus is functionally equivalent to a whole-chromosome aneuploidy, because almost all protein-coding genes on chromosome 14 are coded on the q-arm, distal to the TCRα locus (Fig. 1a). Interestingly, a smaller fraction of the cell population, entailing 0.5–0.9% of the cells, had an apparent gain of chromosome 14 (Fig. 1e,f). This functional chromosome 14 gain is assumed to result from mis-segregation of an acentromeric q-arm[27]. In particular, 100 chromosome 14 genes were underexpressed, and 107 chromosome 14 genes (out of 270 chromosome 14 genes expressed in T cells) were overexpressed in the cells categorized as harboring a chromosome 14 loss or gain, respectively (Extended Data Fig. 1 and Supplementary Table 1). To set a clear statistical threshold for gains and losses, only cells with inferCNV scores >2 standard deviations from the mean score of the population were defined as having a chromosomal aberration (Methods).

Aneuploidy is corroborated by FISH and ddPCR analyses. To corroborate the scRNA-seq results, we next performed FISH assays employing red and green probes proximal and distal to the TCRα

locus on chromosome 14, respectively. Expectedly, most examined nuclei had two foci of co-localized red and green signals (often co-detected as a yellow signal). Notably, in three independent FISH iterations, signal patterns indicative of aneuploidy were observed significantly more frequently in TCRα-targeted cells than in control cells (Fig. 2a,b). These cells had either a single focus of co-localized signals or one focus of co-localized signals and another red focus, interpreted as corresponding to a truncation distal to the targeted gene. In particular, the 4% excess rate of these FISH patterns in TCRα-targeted cells, compared to control cells, is in agreement with the scRNA-seq analysis. The rate of chromosome 14 breakage and its incomplete repair can further be monitored using ddPCR[31] (Fig. 2c). DNA was collected at different timepoints after CRISPR–Cas9 RNP electroporation, to assess the dynamics of dislinkage between the two sides of the break. As early as 3 hours after electroporation, the rate of dislinkage has peaked at more than 45% (Fig. 2d,e). Dislinkage rates were greatly reduced by 24 hours but remained significantly higher in the TCRα-targeted sample compared to the control sample, for at least 11 days, indicating incomplete repair. This ddPCR analysis alone cannot discriminate among transient breaks, translocations and deletions of various sizes, including asymmetrical deletions that span primer/probe binding sites. Still, the ddPCR results are consistent with the results from the scRNA-seq and FISH analyses. Moreover, the ddPCR assay provides a scalable and cost-effective means to track the dynamics of breakage, repair and aberration. Notably, we detected similar rates of aneuploidy and truncations when targeting the TCRα locus with CRISPR–Cas9 and an alternative gRNA or with the alternative nuclease CRISPR–Cas12a (Cpf1 (ref. [32]); Extended Data Fig. 2).

Aneuploid cells have a reduced fitness but are nevertheless detected after prolonged culturing. We next used t-distributed stochastic neighbor embedding (tSNE) analysis to cluster T cells according to their transcriptional signatures (Fig. 3a and Extended Data Fig. 3). We found a similar distribution, among the clusters, of T cells transfected with CRISPR–Cas9 RNPs entailing either the TCRα-targeting gRNA or an irrelevant gRNA with no human target (Fig. 3b). Moreover, among cells receiving the TCRα-targeting gRNA, neither cells with chromosome 14 loss nor cells with chromosome 14 gain were found to be considerably enriched in any T cell subset (Fig. 3c). This implies unbiased incidence of aneuploidy as well as similar selection forces acting on aneuploid cells of various T cell states. However, a gene set enrichment analysis (GSEA) detected significant differences in global gene expression patterns among the groups, beyond the expected reduced expression of the genes encoded on chromosome 14 (Extended Data Fig. 4). Specifically, the transcriptional signatures enriched in T cells with a chromosome 14 loss or gain reflected reduced expression of genes associated with the cell cycle and with various metabolic pathways and increased expression of genes associated with p53 pathway activation and with apoptosis (Fig. 3d–f and Supplementary Table 1). Moreover, a larger fraction of cells with a chromosome 14 loss were found in the G1 cell cycle phase compared to treated cells without an aberration (Fig. 3g). We, thus, hypothesized that longer culturing will reduce the prevalence of aneuploid cells, and we repeated the above experiments comparing the effects of 4 days versus 11 days of T cell culturing after the CRISPR–Cas9 RNP electroporation (Extended Data Fig. 5). Although the aberration rates at day 4 were highly consistent with the results of the previous experiment (Extended Data Fig. 5), scRNA-seq at day 11 showed a marked reduction in the fraction of aneuploid cells (Fig. 3h and Extended Data Fig. 5). The reduced proportion of aneuploid cells is not due to a fitness cost of TCR disruption alone, as the fraction of $CD3^-$ cells remained high (Extended Data Fig. 5). Notably, 0.9% of the T cells were found to have a chromosome 14 loss even after 11 days of culture (Fig. 3h and Extended Data Fig. 5). The persistence of chromosomal aberrations at day 11 was further corroborated by ddPCR (Fig. 2d,e and Extended Data Fig. 5), whereas the sensitivity of FISH analysis for the detection of low aneuploidy rates was insufficient (Extended Data Fig. 5). Finally, both cell cycle phase analysis and GSEA indicated that the aneuploid cells continued to have a reduced fitness at day 11 in comparison to normal cells (Extended Data Figs. 5 and 6 and Supplementary Table 1). Cumulatively, these results indicate that prolonged T cell cultures reduce the risk of transplanting aneuploid cells, but they underscore the need for additional mitigation strategies.

Targeting different loci concomitantly with several gRNAs aggravates the risk for chromosomal aberrations. Stadtmauer et al.[6] identified multiple translocations between cleaved chromosomes when co-delivering three gRNAs targeting both TCR loci as well as the PDCD1 gene. We, therefore, used the same gRNA combination for CRISPR–Cas9 RNP electroporation of primary human T cells (Fig. 4a). We verified cleavage efficiency (Extended Data Fig. 7) and performed scRNA-seq to analyze gene expression patterns and infer copy number changes along the targeted chromosomes. The transcriptional downregulation of TCRα, TCRβ and PDCD1 was confirmed (Fig. 4b and Extended Data Fig. 7). Notably, in this experiment, we found expression patterns indicative of a chromosome 14 loss and gain in 9.0% and 1.4% of the cells, respectively (Fig. 4c,d and Extended Data Fig. 8). Strikingly, we further found as many as 9.9% of treated cells to be characterized with chromosome 7 truncations, entailing the TCRβ locus (Fig. 4c,d). Interestingly, the extent of the detected aberrations is in good agreement with the chromosomal position of the cleavage sites: cleaving the TCRα locus, near the chromosome 14 centromere, leads to loss of the entire arm and to functional whole-chromosome aneuploidy; cleaving the TCRβ locus, in the middle of the chromosome 7 q-arm, leads to the expected truncations; and cleaving the PDCD1 gene, which resides near the chromosome 2 q-arm telomere, expectedly has a lesser effect on copy number and gene expression (Extended Data Fig. 8). Finally, a GSEA confirmed the transcriptional differences observed in our first experiment in cells that have lost or gained chromosome 14 and identified very similar pathway enrichments in the cells with a chromosome 7 truncation (Fig. 4e–g, Extended Data Fig. 9 and Supplementary Table 1). We did not culture the cells for more than 4 days after multiplex editing, but our data imply that such cultures would show a negative selection against truncated and aneuploid cells, in concordance with cells edited only at the *TRAC* locus (Fig. 3h and Extended Data Fig. 5).

Discussion

Aneuploidy is associated with most types of cancers[33]. Of note, chromosome 14 loss is frequently found in early-onset colon cancer[34] and is among the most commonly affected chromosomal regions in ovarian cancer[35]. Chromosome 14 monosomy, trisomy and tetrasomy are also frequently found in meningioma[36]. Similarly, high-grade glioma[37] and adult T cell leukemia and lymphoma[38] are often characterized by chromosome 7 trisomy, whereas chromosome 14 monosomies and tetrasomies are not frequent events in T cell malignancies. To date, no serious adverse events in clinical trials have been attributed to genome editing. However, our findings raise the possibility that Cas9-induced aneuploidy and chromosomal truncations might be associated with increased risk of tumorigenesis. The methods we described were optimized for the detection of aneuploidy and large truncations, therefore underestimating the overall occurrence of genetic alterations. Although detected in some cases (Fig. 2a), translocations and focal deletions may better be assessed using complementary technologies[6].

We describe high aberration rates induced by different nucleases and different gRNAs. It is possible that optimizing the electroporation conditions, or using a clinical-grade electroporator, may reduce

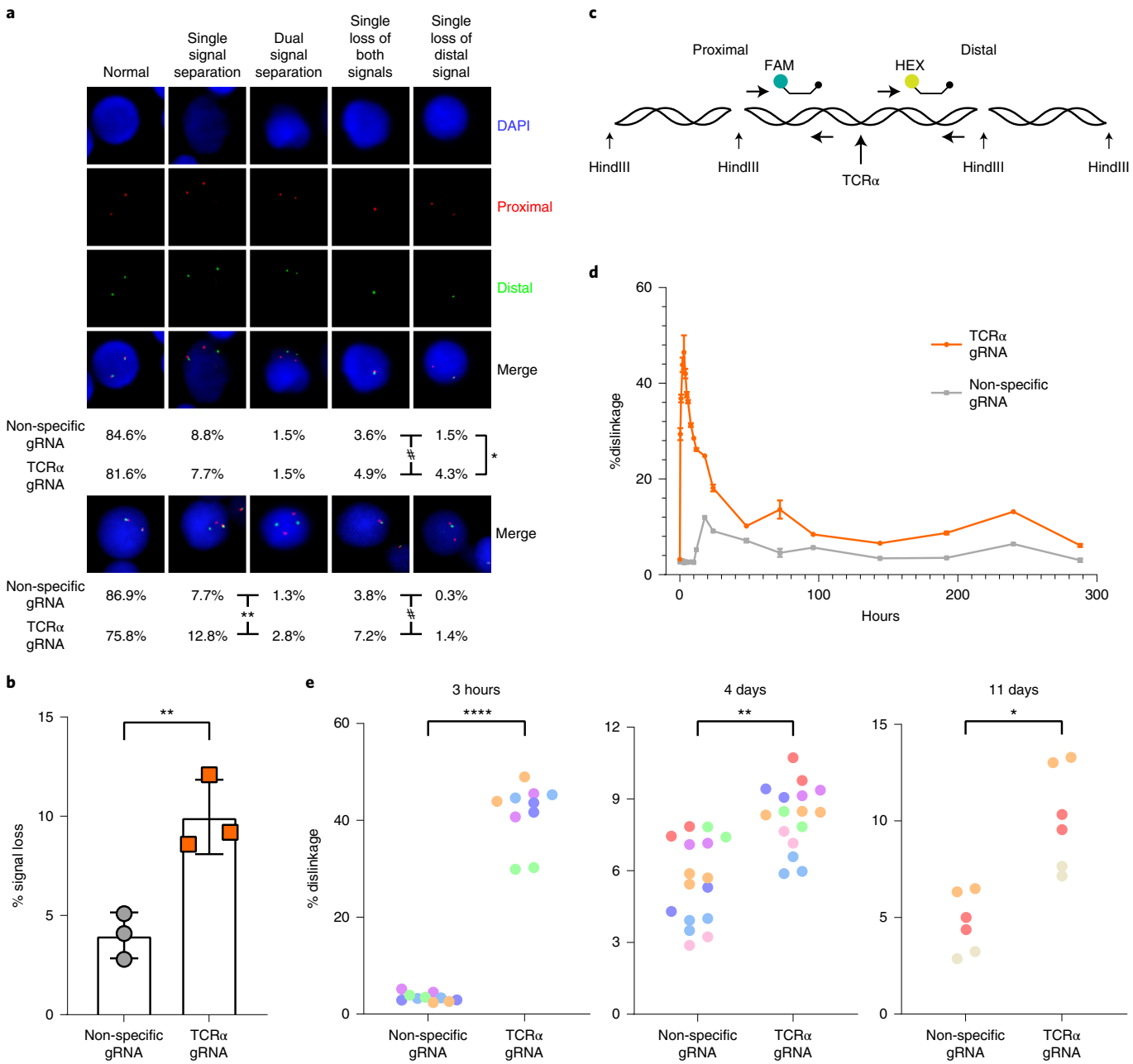

Fig. 2 | FISH and ddPCR analyses of chromosome 14 aberrations. a, FISH analysis of cells treated with either a non-specific or a TCRα-targeting gRNA. In the pictures are examples of all signal patterns found among analyzed cells. The frequency of each signal pattern, among cells electroporated with the TCRα-targeting gRNA or a non-specific gRNA, is presented below the pictures. In a first experiment (top), $n=273$ and $n=506$ for cells electroporated with a non-specific and TCRα-targeting gRNA, respectively; $^{*}P=0.0129$, Fisher's exact test for loss of distal signal comparison, and $\#P=0.0486$, Fisher's exact test for loss of either both signals or only the distal signal. In a second experiment (bottom), $n=313$ and $n=360$ for cells electroporated with a non-specific and TCRα-targeting gRNA, respectively; $\#P=0.0115$, Fisher's exact test for loss of either both signals or the distal signal, and $^{**}P=0.0048$ for either single or dual signal separation for the second experiment. **b**, Quantification of **a**. From three independent experiments, 4 days after electroporation. Signal loss designates loss of either both signals or only the distal signal. Mean and standard deviations are indicated. $^{**}P=0.0093$, two-sided unpaired *t*-test. **c**, Schematic depiction of the ddPCR experiment. Genomic DNA is sheared using the HindIII restriction enzyme. The two sets of primers and probe are on the same restriction fragment and are separated only upon CRISPR–Cas9 cleavage. **d**, Dislinkage, calculated based on the rate of single and dual color droplets (Methods), is analyzed at different timepoints after CRISPR–Cas9 electroporation with either a TCRα-targeting gRNA (orange) or a non-specific (gray) gRNA from a single experiment. Mean and standard deviation for technical replicates are indicated. **e**, Dislinkage at 3 hours (left), 4 days (middle) or 11 days (right) after CRISPR–Cas9 electroporation. Each color represents a different human donor. Each dot represents a technical replication. $n=3$–7, $^{****}P<0.0001$ and $^{*}P=0.0085$, $^{*}P=0.0474$, two-sided unpaired *t*-test.

the aberration frequency, by affecting the re-cutting rate of repaired double-strand breaks. Better yet, aberration rates can be reduced by using base editors instead of nucleases[39,40]. In the liver, gene insertion by homologous recombination can be achieved without nucleases[41–43]. However, in T cells, nucleases may still be required for site-specific gene insertion of CAR and engineered TCR genes into

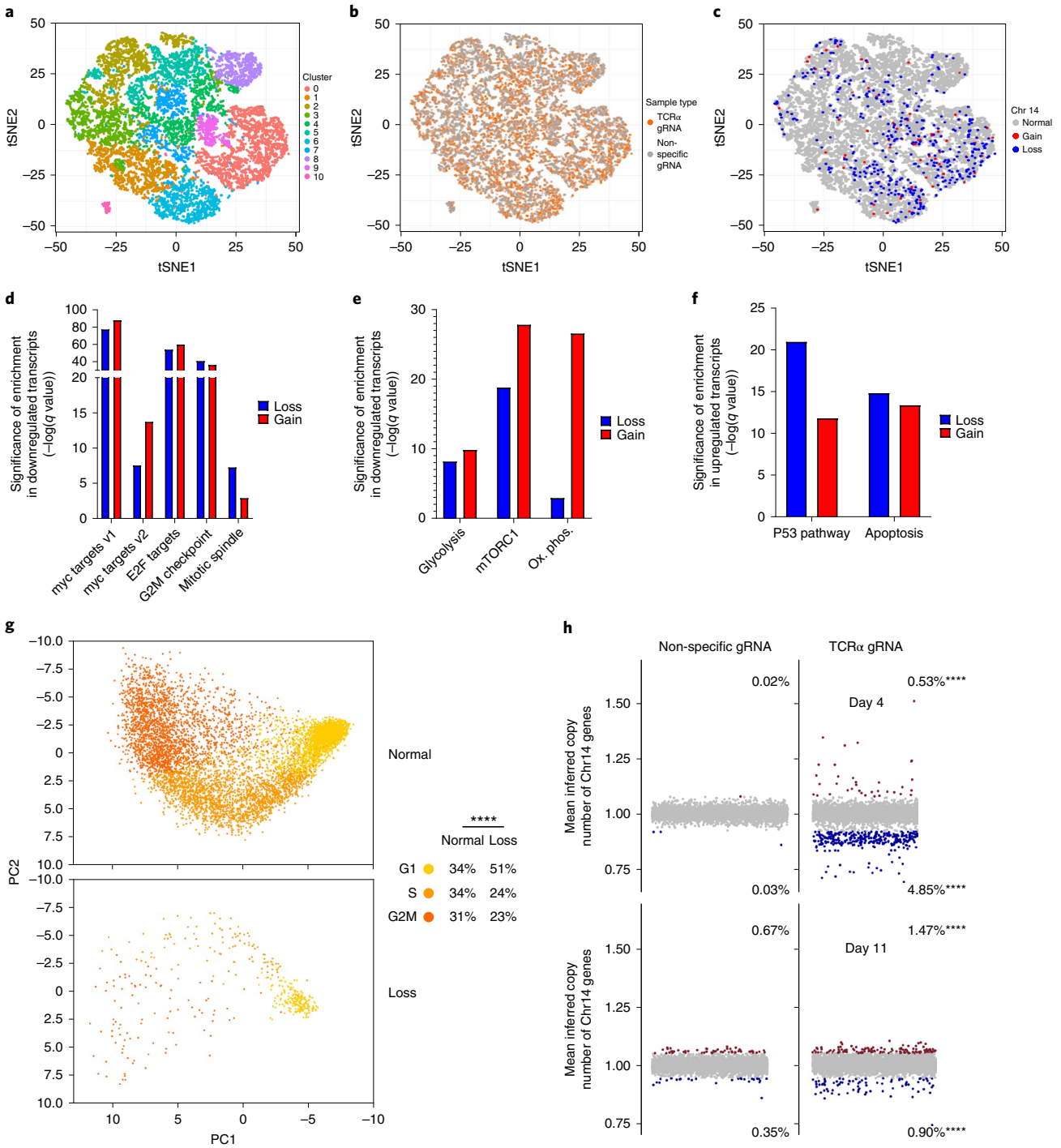

Fig. 3 | Global gene expression analysis after genome editing. a, scRNA-seq data from primary human T cells showing 13,755 cells as individual dots. Data are displayed by tSNE with each cluster colored differently. **b**, Distribution of cells electroporated with a non-specific (gray) or TCRα-targeting (orange) gRNA among the clusters. **c**, Distribution of cells with a chromosome 14 loss (blue) or gain (red) among the clusters. **d**–**f**, GSEA for 'hallmark' gene sets associated with cell cycle (**d**), metabolism (**e**) and p53 expression and apoptosis (**f**) in cells with chromosome 14 loss (blue) and or gain (red). **g**, Principal component (PC) analysis of cell cycle phase among cells treated with a TCRα-targeting gRNAs and characterized, as in Fig. 1f, as having a chromosome 14 loss (bottom) or not (normal, up). Legend and fraction of cells in each cell cycle phase are indicated on the right. ****$P < 0.0001$, Fisher's exact test for G1 phase compared to S/G2M phases. $n = 7,289$ and $n = 411$ for cells without or with a chromosome 14 loss, respectively. **h**, Each dot represents the mean inferred copy number of genes coded on chromosome 14 in each cell treated with a non-specific gRNA (left) or a TCRα-targeting gRNA (right). Cells are marked with dots spread along the *x* axis. The dots are colored red and blue when corresponding to cells with a chromosome 14 gain or loss, respectively, if their mean inferred gene copy number is >3 standard deviations (dark blue and dark red) from the population's mean. For day 4, $n = 8,642$ and $n = 6,592$ for cells transfected with a non-specific (left) or TCRα-targeting (right) gRNA, respectively. For day 11, $n = 8,642$ and $n = 9,197$ for cells transfected with a non-specific (left) or TCRα-targeting (right) gRNA, respectively. The expression levels in cells treated with a non-specific gRNA 4 days after CRISPR–Cas9 electroporation served as a reference in both analyses. ****$P < 0.0001$, Fisher's exact test comparing chromosome 14 gain or loss between cells treated with the TCRα gRNA and cells treated with a non-specific gRNA.

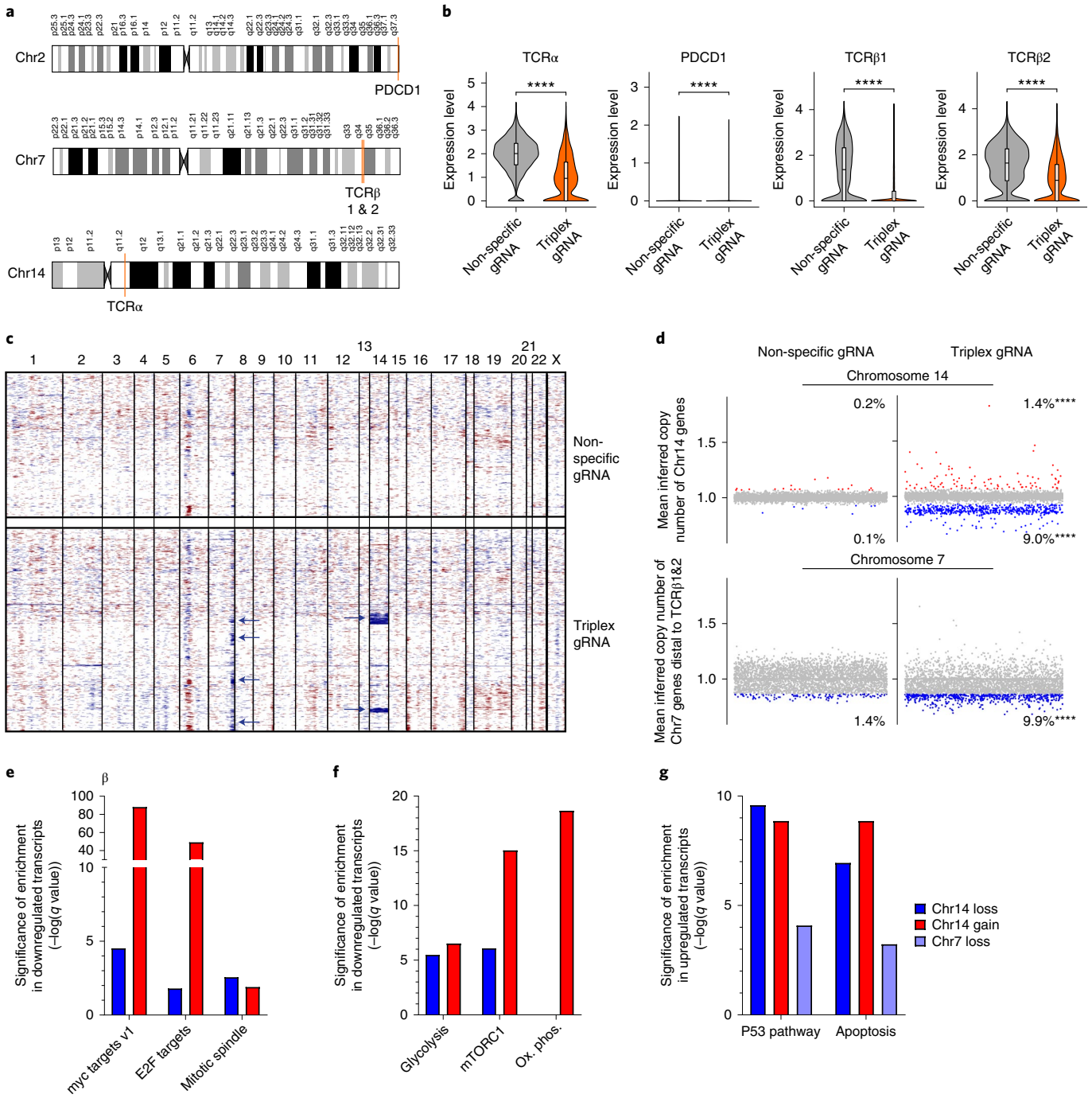

Fig. 4 | Targeting different loci concomitantly with several gRNAs aggravates chromosomal aberrations. a, Schematic depiction of human chromosomes 2, 7 and 14. Target loci are shown in orange. A single gRNA targets both TCRβ1 and TCRβ2. **b**, RNA expression of TCRα, PDCD1, TCRβ1 and TCRβ2 in cells treated with either a non-specific gRNA or a combination of TCRα-targeting, TCRβs-targeting and PDCD1-targeting gRNAs. ****$P < 0.0001$, two-sided unpaired Wilcoxon test. **c**, Heat map depicting gene copy numbers inferred from scRNA-seq analysis after treatment with either a non-specific gRNA or a combination of TCRα-targeting, TCRβs-targeting and PDCD1-targeting gRNAs. Each line represents an individual cell. The chromosomes are ordered in columns, and the color coding indicates an increase (red) or decrease (blue) in copy number. Blue arrows indicate loss of chromosome 14 or chromosome 7 segments. **d**, Each dot represents the mean inferred copy number of genes coded on the relevant chromosome in each cell treated with a non-specific gRNA (left), the combination of TCRα-targeting, TCRβs-targeting and PDCD1-targeting gRNAs (right). For chromosome 7, the mean inferred copy number of genes coded distal to TCRβ1 and TCRβ2 is analyzed. Cells are marked with dots spread along the *x* axis. The dots are colored red and blue when corresponding to cells with a chromosome 14 gain or loss, respectively, if their mean inferred gene copy number is >2 standard deviations away from the population's mean. $n = 8{,}619$ and $n = 6{,}326$ for cells treated with a non-specific gRNA (left) or a combination of TCRα-targeting, TCRβs-targeting and PDCD1-targeting gRNAs (right), respectively. ****$P < 0.0001$, Fisher's exact test comparing chromosome gain or loss between cells treated with the TCRα/β gRNA and cells treated with a non-specific gRNA. **e**–**g**, GSEA of 'hallmark' gene sets associated with cell cycle (**e**), metabolism (**f**) and p53 expression and apoptosis (**g**) in cells with chromosome 14 loss (blue) and in cells with chromosome 14 gain (red).

TCR loci to enhance T cell potency and delay exhaustion[8–10]. Further studies are required to determine whether sorting for expression of the targeted receptor cassette will help reduce the rate of cells with nuclease-induced aberrations. Alternatively, endogenous genes that are differentially expressed in aberrant T cells may be used for cell sorting before adoptive transfer. As a first step toward this aim, we compiled a list of genes whose expression significantly differed between the cells that have lost chromosome 14 and those that have not (Supplementary Table 1), and we manually curated the list to identify cell surface proteins. However, our initial attempts to sort against markers of aneuploidy only mildly reduced the aberration rate (Extended Data Fig. 10). Finally, our GSEA suggests that aneuploidy provides fitness disadvantage to the T cells in vitro (Fig. 3d–h, Supplementary Table 1 and Extended Data Fig. 5), in line with multiple studies that showed the negative effect of aneuploidy on cell survival and proliferation[33,44,45]. Indeed, prolonged culturing has reduced the prevalence of aneuploid cells and could be considered in clinical protocols, while also weighing the effects on cell activation, differentiation and exhaustion.

In conclusion, inferring copy number alterations from scRNA-seq data is an unbiased, high-throughput method to identify nuclease-induced chromosomal aberrations. Our discovery of frequent aneuploidy and chromosomal truncations in human T cells targeted using CRISPR–Cas9 and clinical gRNA sequences highlights potential oncogenic risks and underscores the need for mitigation strategies to allow the safe application of nucleases in adoptive T cell transfer and beyond.

Online content

Any methods, additional references, Nature Research reporting summaries, source data, extended data, supplementary information, acknowledgements, peer review information; details of author contributions and competing interests; and statements of data and code availability are available at https://doi.org/10.1038/s41587-022-01377-0.

Received: 18 August 2021; Accepted: 31 May 2022;
Published online: 30 June 2022

References

1. Weber, E. W., Maus, M. V. & Mackall, C. L. The emerging landscape of immune cell therapies. *Cell* **181**, 46–62 (2020).
2. MacLeod, D. T. et al. Integration of a CD19 CAR into the TCR alpha chain locus streamlines production of allogeneic gene-edited CAR T cells. *Mol. Ther.* **25**, 949–961 (2017).
3. Philip, L. P. B. et al. Multiplex genome-edited T-cell manufacturing platform for 'off-the-shelf' adoptive T-cell immunotherapies. *Cancer Res.* **75**, 3853–3864 (2015).
4. Qasim, W. et al. Molecular remission of infant B-ALL after infusion of universal TALEN gene-edited CAR T cells. *Sci. Transl. Med.* **9**, 1–10 (2017).
5. Osborn, M. J. et al. Evaluation of TCR gene editing achieved by TALENs, CRISPR/Cas9, and megaTAL nucleases. *Mol. Ther.* **24**, 570–581 (2016).
6. Stadtmauer, E. A. et al. CRISPR-engineered T cells in patients with refractory cancer. *Science* **367**, eaba7365 (2020).
7. Braendstrup, P., Levine, B. L. & Ruella, M. The long road to the first FDA-approved gene therapy: chimeric antigen receptor T cells targeting CD19. *Cytotherapy* **22**, 57–69 (2020).
8. Eyquem, J. et al. Targeting a CAR to the *TRAC* locus with CRISPR/Cas9 enhances tumour rejection. *Nature* **543**, 113–117 (2017).
9. Roth, T. L. et al. Reprogramming human T cell function and specificity with non-viral genome targeting. *Nature* **559**, 405–409 (2018).
10. Schober, K. et al. Orthotopic replacement of T-cell receptor α- and β-chains with preservation of near-physiological T-cell function. *Nat. Biomed. Eng.* **3**, 977–984 (2019).
11. Mansilla-Soto, J. et al. HLA-independent T cell receptors for targeting tumors with low antigen density. *Nat. Med.* **28**, 345–352 (2022).
12. Shifrut, E. et al. Genome-wide CRISPR screens in primary human T cells reveal key regulators of immune function. *Cell* **175**, 1958–1971 (2018).
13. Valton, J. et al. A multidrug-resistant engineered CAR T cell for allogeneic combination immunotherapy. *Mol. Ther.* **23**, 1507–1518 (2015).
14. Rupp, L. J. et al. CRISPR/Cas9-mediated PD-1 disruption enhances anti-tumor efficacy of human chimeric antigen receptor T cells. *Sci Rep.* **7**, 737 (2017).
15. Nahmad, A. D. et al. Engineered B cells expressing an anti-HIV antibody enable memory retention, isotype switching and clonal expansion. *Nat. Commun.* **17**, 5851 (2020).
16. Charlesworth, C. T. et al. Identification of preexisting adaptive immunity to Cas9 proteins in humans. *Nat. Med.* **25**, 249–254 (2019).
17. Enache, O. M. et al. Cas9 activates the p53 pathway and selects for p53-inactivating mutations. *Nat. Genet.* **52**, 662–668 (2020).
18. Lazzarotto, C. R. et al. CHANGE-seq reveals genetic and epigenetic effects on CRISPR–Cas9 genome-wide activity. *Nat. Biotechnol.* **38**, 1317–1327 (2020).
19. Adikusuma, F. et al. Large deletions induced by Cas9 cleavage. *Nature* **560**, E8–E9 (2018).
20. Papathanasiou, S. et al. Whole chromosome loss and genomic instability in mouse embryos after CRISPR–Cas9 genome editing. *Nat. Commun.* **12**, 5855 (2021).
21. Alanis-lobato, G., Zohren, J., Mccarthy, A., Fogarty, N. M. E. & Kubikova, N. Frequent loss-of-heterozygosity in CRISPR–Cas9-edited early human embryos. *Proc. Natl Acad. Sci. USA* **118**, e2004832117 (2021).
22. Weisheit, I. et al. Detection of deleterious on-target effects after HDR-mediated CRISPR editing. *Cell Rep.* **31**, 107689 (2020).
23. Boutin, J. et al. CRISPR–Cas9 globin editing can induce megabase-scale copy-neutral losses of heterozygosity in hematopoietic cells. *Nat. Commun.* **12**, 4922 (2021).
24. Przewrocka, J., Rowan, A., Rosenthal, R., Kanu, N. & Swanton, C. Unintended on-target chromosomal instability following CRISPR/Cas9 single gene targeting. *Ann. Oncol.* **31**, 1270–1273 (2020).
25. Kosicki, M., Tomberg, K. & Bradley, A. Repair of double-strand breaks induced by CRISPR–Cas9 leads to large deletions and complex rearrangements. *Nat. Biotechnol.* **36**, 765–771 (2018).
26. Zuccaro, M. V. et al. Allele-specific chromosome removal after Cas9 cleavage in human embryos. *Cell* **183**, 1650–1664 (2020).
27. Leibowitz, M. L. et al. Chromothripsis as an on-target consequence of CRISPR–Cas9 genome editing. *Nat. Genet.* **53**, 895–905 (2021).
28. Urnov, F. D. CRISPR–Cas9 can cause chromothripsis. *Nat. Genet.* **53**, 765–769 (2021).
29. Patel, A. P. et al. Single-cell RNA-seq highlights intratumoral heterogeneity in primary glioblastoma. *Science* **344**, 1396–1402 (2014).
30. Tirosh, I. et al. Dissecting the multicellular ecosystem of metastatic melanoma by single-cell RNA-seq. *Science* **352**, 189–196 (2016).
31. Puig, M. et al. Determining the impact of uncharacterized inversions in the human genome by droplet digital PCR. *Genome Res.* **30**, 724–735 (2020).
32. Zetsche, B. et al. Cpf1 is a single RNA-guided endonuclease of a class 2 CRISPR–Cas system. *Cell* **163**, 759–771 (2015).
33. Ben-David, U. & Amon, A. Context is everything: aneuploidy in cancer. *Nat. Rev. Genet.* **21**, 44–62 (2020).
34. Mourra, N. et al. High frequency of chromosome 14 deletion in early-onset colon cancer. *Dis. Colon Rectum* **50**, 1881–1886 (2007).
35. Bandera, C. A. et al. Deletion mapping of two potential chromosome 14 tumor suppressor gene loci in ovarian carcinoma. *Cancer Res.* **57**, 513–516 (1997).
36. Tabernero, M. D. et al. Characterization of chromosome 14 abnormalities by interphase in situ hybridization and comparative genomic hybridization in 124 meningiomas. *Am. J. Clin. Pathol.* **123**, 744–751 (2005).
37. Lopez-Gines, C. et al. Association of chromosome 7, chromosome 10 and EGFR gene amplification in glioblastoma multiforme. *Clin. Neuropathol.* **24**, 209–218 (2005).
38. Kamada, N. et al. Chromosome abnormalities in adult T-cell leukemia/lymphoma: a karyotype review committee report. *Cancer Res.* **52**, 1481–1493 (1992).
39. Webber, B. R. et al. Highly efficient multiplex human T cell engineering without double-strand breaks using Cas9 base editors. Nat. Commun. 10, 5222 (2019).
40. Anzalone, A. V., Koblan, L. W. & Liu, D. R. Genome editing with CRISPR–Cas nucleases, base editors, transposases and prime editors. *Nat. Biotechnol.* **38**, 824–844 (2020).
41. Barzel, A. et al. Promoterless gene targeting without nucleases ameliorates haemophilia B in mice. *Nature* **517**, 360–364 (2015).
42. Porro, F. et al. Promoterless gene targeting without nucleases rescues lethality of a Crigler–Najjar syndrome mouse model. *EMBO Mol. Med.* **9**, 1346–1355 (2017).
43. Chandler, R. J. et al. Promoterless, nuclease- free genome editing confers a growth advantage for corrected hepatocytes in mice with methylmalonic acidemia. *Hepatology* **73**, 2223–2237 (2021).
44. Rutledge, S. D. et al. Selective advantage of trisomic human cells cultured in non-standard conditions. *Sci Rep.* **6**, 22828 (2016).
45. Sheltzer, J. M. et al. Single-chromosome gains commonly function as tumor suppressors. *Cancer Cell* **31**, 240–255 (2017).

Methods

T cell editing. Whole blood was obtained with donor consent from the Israeli Blood Bank (Magen David Adom, Sheiba Medical Center) in accordance with the Tel Aviv University Review Board. Peripheral blood mononuclear cells were extracted using Lymphocyte Separation Medium (MP Biomedicals) and cryopreserved until subsequent use. After thawing, cells were activated for 24–48 hours with 1 μg ml^{-1} of anti-human CD28 (BioGems) and anti-human CD3 (BioGems). Cells were cultured in MEM-Alpha (Biological Industries) supplemented with 10% heat-inactivated FCS (Sigma-Aldrich), 50 IU of rhIL-2 (PeproTech) and penicillin–streptomycin.

For RNP electroporation, 18 pmol of Alt-R spCas9 Nuclease V3 (Integrated DNA Technologies (IDT)) and 66 pmol of Alt-R CRISPR–Cas9 gRNA (IDT) per 1×10^6 cells per target were complexed in Buffer T (IDT). In experiments involving a triple target (TCRα, TCRβ and PD-1), quantities of Cas9:gRNA complexes were tripled for a non-specific control. For experiments aiming at reducing the aneuploid cell fraction, we used Alt-R sp HiFi Cas9 Nuclease V3 (IDT). For experiments involving CRISPR–Cas12a, Alt-R L.b. Cas12a (Cpf1) Ultra (IDT) and CRISPR RNA (crRNA) were used at mass ratios equivalent to those used in Cas9 electroporations, when 1×10^6 cells per target were complexed in Buffer T (IDT). gRNA and crRNA sequences are provided in Supplementary Table 1. Cells were harvested, washed and electroporated at 1,600 V, 10 ms, three pulses in 10 μl of Buffer T and subsequently grown in culture media devoid of P/S. For prolonged culture, live cells were purified using Lymphocyte Separation Medium (MP Biomedicals) every other day.

Flow cytometry. Cells were harvested, washed and resuspended in Cell Staining Buffer (BioLegend) containing 1/100 diluted anti-human CD3 or anti-human TCRα/β (BioLegend), both targeting the TCR complex. Staining was performed for 15 minutes at room temperature in the dark. Finally, cells were washed, and data acquisition was performed on an Attune NxT Flow Cytometer (Life Technologies).

Fluorescence-activated cell sorting. Cell sorting was performed 3 days after electroporation. Cells were harvested, washed and resuspended in PBS supplemented with 5% BSA containing 1/100 diluted anti-human CD70 and anti-human CD52 (BioLegend). Staining was performed for 15 minutes at room temperature in the dark. Subsequently, cells were washed and resuspended in PBS supplemented with 0.5% BSA. During fluorescence-activated cell sorting (FACS), cells were collected in MEM-Alpha (Biological Industries) supplemented with 0.5% heat-inactivated FCS (Sigma-Aldrich) and P/S. Acquisition was performed on a FACSAria III (BD Biosciences). After collection, live cells were purified using Lymphocyte Separation Medium (MP Biomedicals), washed and cultured in MEM-Alpha (Biological Industries) supplemented with 10% heat-inactivated FCS (Sigma-Aldrich), 50 IU of rhIL-2 (PeproTech) and P/S. Purity of the sorted cells can be found in Extended Data Fig. 10.

scRNA-seq. Edited T cells were harvested and live cells were purified using Lymphocyte Separation Medium (MP Biomedicals), washed and resuspended in PBS supplemented with 0.5% BSA to achieve optimal concentration of approximately 1,000 cells per microliter. Cells were counted and viability assessed manually in trypan blue 0.4% (Biological Industries). In total, 17,000 cells were loaded on Next GEM Chip (10x Genomics). Libraries were prepared at the Single-Cell Genomics Core, Faculty of Medicine, Tel Aviv University, using the 10x Genomics Chromium Controller in conjunction with the single-cell 3′ version 3.1 kit, protocol revision D. cDNA synthesis, barcoding and library preparation were then carried out according to the manufacturer's instructions. In brief, cDNA amplification was performed for 11 cycles. Sample index PCR was performed for 13 cycles using Chromium i7 Sample Indices. Resulting libraries were quantified and analyzed by Qubit and TapeStation. Libraries were sequenced on the NextSeq 500 platform (Illumina), following the manufacturer's protocol, using a NextSeq 500/550 High Output Kit version 2.5 (75 cycles) (Illumina). Sequencing was performed at the Genomics Research Unit at the Life Sciences Inter-Departmental Research Facility Unit, Tel Aviv University.

scRNA-seq gene expression pre-processing. Raw BCL files for the DNA sequencing data were processed using Cell Ranger DNA (version 5.0.1). Data were aligned to the 10x Genomics GRCh38 genome. Results were visualized in the Loupe scDNA Browser (version 5.0.0). Raw gene expression data were extracted from the Seurat object as recommended in the 'Using 10x data' section (inferCNV of the Trinity CTAT Project, https://github.com/broadinstitute/inferCNV).

inferCNV. inferCNV was used to infer copy number changes from the gene expression profiles[29,30] The non-targeted T cell population was used as the reference, and the CRISPR–Cas9-targeted population was tested, with the following parameters: 'denoise', default hidden Markov model (HMM) settings and a value of 0.1 for 'cutoff'.

Identification of aberrant cells. For each cell, the mean of inferCNV scores was calculated across genes and plotted. The PDCD1 gene resides near the chromosome 2 q-arm telomere, and only 15 genes, expressed in T cells, reside between the TCRα gene and the chromosome 14 centromere. Therefore, for chromosome 14 and chromosome 2, all of the expressed genes on the respective chromosomes were used for the analysis. For chromosome 7, the 47 expressed genes that reside distal to TCRβ were used. Cells with a mean lower or higher >2 standard deviations from the mean of the population were determined as cells with a loss or a gain, respectively.

Simulation analysis for downregulated genes. To determine whether cells categorized as harboring a chromosome 14 loss of a chr7 distal loss also had a significant increase in the fraction of zero expression calls (that is, whether these regions are enriched with genes not detected at all by scRNA-seq), the ratio between the number of genes from each chromosome with expression = 0 and expression > 0 for each cell population (loss versus non-loss) was calculated. The fold change (FC) of the proportion of zero calls between the normal and aberrant cells was determined, and 10,000 simulations were then performed, selecting an equivalent number of random genes from other chromosomes. An empirical *P* value was determined by comparing the empirical values to the simulated values.

Differential gene expression analysis. The 'FindMarkers' package from the Seurat library[46] was used to detect the differentially expressed (DE) genes between two groups of cells (logFC of 0.25). The function receives two identities of clusters in the dataset and a value for the minimum percentage that is required for a feature to be detected in either of the two groups of cells. The minimum percentage value that we used is 0.25, and *P* values were calculated using the Wilcoxon test.

The first comparison was made to detect DE genes between the cells that have undergone loss in the TCRα gRNA and the cells that did not show loss or gain in the same treatment group. The second was to detect DE genes between the cell that have undergone gain in the TCRα gRNA and the cells that did not show gain or loss in the same treatment group.

GSEA. The lists of DE genes between each two conditions were determined using Seurat as described above. These lists were subjected to GSEA using the GSEA Molecular Signatures Database (MSigDB) portal (https://www.gsea-msigdb.org/gsea/msigdb/). The analysis was run using the following curated gene sets: 'hallmark', 'KEGG', 'GO biological process' and 'positional' gene sets from the MSigDB[47–49].

ddPCR. For ddPCR, whole genomic DNA was extracted from cells using Gentra PureGene Tissue Kit (Qiagen). To remove sheared genomic fragments, resulting eluates were further purified using AMPure XP beads (Beckman Coulter) at a 0.5:1 ratio. DNA fragmentation by digestion was performed in reaction, using 66 ng of purified genomic DNA and 10 U of HindIII-HF (New England Biolabs) in ddPCR Supermix for Probes (Bio-Rad). Thermocycling reaction was performed as per manufacturer recommendations. Sequences for the primers and probes can be found in Supplementary Table 1. Reactions were performed using a QX200 Droplet Digital PCR System (Bio-Rad). To analyze for dislinkage, we used the following equation as per the resulting QuantaSoft (Bio-Rad) Linkage (*Linkage*) and Concentration (C_{HEX} and C_{FAM}) values:

$$\%Dislinkage = 100 - \left(\frac{Linkage}{\frac{C_{HEX}+C_{FAM}}{2}} x100\right)$$

For dislinkage follow-up, multiple electroporations of treated cells were pooled and then divided in separate wells for collection at each timepoint. Cells were seeded at 1×10^6 cells per milliliter in MEM-Alpha (Biological Industries) supplemented with 10% heat-inactivated FCS (Sigma-Aldrich) and 50 IU of rhIL-2 (PeproTech).

Nucleic acid manipulations. For T7 endonuclease 1 (T7E1) assays, PCR amplification was performed on Gentra PureGene Tissue Kit (Qiagen) extracted genomic DNA. Then, 200–500 ng of genomic DNA was amplified using PrimeStar MAX (Takara) for 35 cycles. Primers for these reactions can be found in Supplementary Table 1. Resulting amplicons were denatured and reannealed in a thermocycler before nuclease reaction using T7E1 (New England Biolabs) at 37 °C for 20 minutes. Resulting fragments were analyzed by agarose gel electrophoresis and quantified using Bio-Vision (Vilber Lourmat) using a rolling ball for background subtraction. Efficiency was calculated using the following equation:

$$Cleavage\ efficiency = 100 \times \left(1 - \left(1 - fraction\ cleaved\right)^{\frac{1}{2}}\right)$$

For TIDE analysis, PCR amplicons were subjected to purification by AMPure XP beads (Beckman Coulter) at a 1:1 ratio. Sanger sequencing was performed at the DNA Sequencing Unit, Tel Aviv University. Samples were compared using TIDE (https://tide.nki.nl/)[50].

FISH. FISH analysis was performed following the manufacturer's instructions (Cytocell) on interphase human T cells from peripheral blood spreads using the TRACD breakapart probe. Images were captured using GenASIs imaging system.

Statistics. For FISH, genomic DNA cleavage efficiency and flow cytometry knock-out efficiency, statistical analyses were performed in Prism (GraphPad). For *t*-tests on dislinkage by ddPCR, for each donor technical replicates were averaged, and *t*-test was performed on the averaged values. Each figure legend denotes the statistic used, central tendency and error bars.

Reporting summary. Further information on research design is available in the Nature Research Reporting Summary linked to this article.

Data availability

All datasets are available within the article and its Supplementary Information. 10x scRNA-seq data have been deposited to the Sequence Read Archive with BioProject accession number PRJNA759387.
Supplementary information and extended data figures are available for this paper. Source data are provided with this paper.

Code availability

The software programs used for individual and integrated analyses are described and referenced in the individual sections in the Methods.

References

46. Stuart, T. et al. Comprehensive integration of single-cell data resource comprehensive integration of single-cell data. *Cell* **177**, 1888–1902 (2019).
47. Liberzon, A. et al. The Molecular Signatures Database (MSigDB) hallmark gene set collection. *Cell Syst.* **1**, 417–425 (2015).
48. Subramanian, A. et al. Gene set enrichment analysis: a knowledge-based approach for interpreting genome-wide expression profiles. *Proc. Natl Acad. Sci. USA* **102**, 15545–15550 (2005).
49. Liberzon, A. et al. Molecular Signatures Database (MSigDB) 3.0. *Bioinformatics* **27**, 1739–1740 (2011).
50. Brinkman, E. K., Chen, T., Amendola, M. & Van Steensel, B. Easy quantitative assessment of genome editing by sequence trace decomposition. *Nucleic Acids Res.* **42**, 1–8 (2014).

Acknowledgements

We thank N. Zelikson (Tel Aviv University) for helpful discussions and for reviewing the manuscript. We thank R. Elkon for computational support. We thank the IDRFU, GRU and SICF units, Tel Aviv University, for logistic support and counsel. This research was funded by a Boaz and Varda Dotan donation (A.B.); H2020 European Research Council grant 759296 570 (A.B.); Israel Science Foundation grants 1632/16, 2157/16 and 2876/21 (A.B.); Israeli Health Ministry grant 0604216191 (A.B.); and National Institutes of Health grant R01 AI167003-01 (A.B.) This research was funded by the European Research Council (759296 to A.B. and 945674 to U.B.-D.); the Gertner Institute Scholarship; the Yoran Institute Scholarship; the SAIA Foundation (A.D.N.); SCGC Tel Aviv University (A.B. and U.B.-D.); the Israel Cancer Research Foundation Development Award (A.M.); the Israel Cancer Research Foundation Gesher Award (U.B.-D.); the Azrieli Faculty Fellowship (U.B.-D.); the Alon Fellowship for Outstanding Young Scientists; the Israel Council for Higher Education (A.M.); and the Edmond J. Safra Center Fellowship for Bioinformatics at Tel Aviv University (E.G.).

Author contributions

A.D.N. designed, performed and analyzed the experiments. E.R. and E.G. analyzed the single-cell RNA sequencing data. T.T. and M.L. performed fluorescence in situ hybridization. M.H.-F. helped with sample culturing and processing. R.K. and H.K. performed single-cell RNA sequencing. E.R. supervised fluorescence in situ hybridization. A.M. and U.B.-D. supervised single-cell RNA sequencing analysis. A.D.N. and A.B. drafted the manuscript and revised it together with A.M. and U.B.-D. U.B.-D. and A.B. supervised the study. A.B. conceptualized the study.

Competing interests

A.B. is a co-founder and an inventor of the underlying patents for LogicBio Therapeutics, developing CRISPR-free genome editing. A.D.N. and A.B. are co-founders and inventors of the underlying patents for Tabby Therapeutics, using CRISPR–Cas9 for B cell engineering. A.D.N. and A.B. hold equity and receive monetary compensation from Tabby Therapeutics. E.R. is an employee of Future Meat Technologies.

Additional information

Extended data is available for this paper at https://doi.org/10.1038/s41587-022-01377-0.

Supplementary information The online version contains supplementary material available at https://doi.org/10.1038/s41587-022-01377-0.

Correspondence and requests for materials should be addressed to Asaf Madi, Uri Ben-David or Adi Barzel.

Peer review information *Nature Biotechnology* thanks Fyodor Urnov and the other, anonymous, reviewer(s) for their contribution to the peer review of this work.

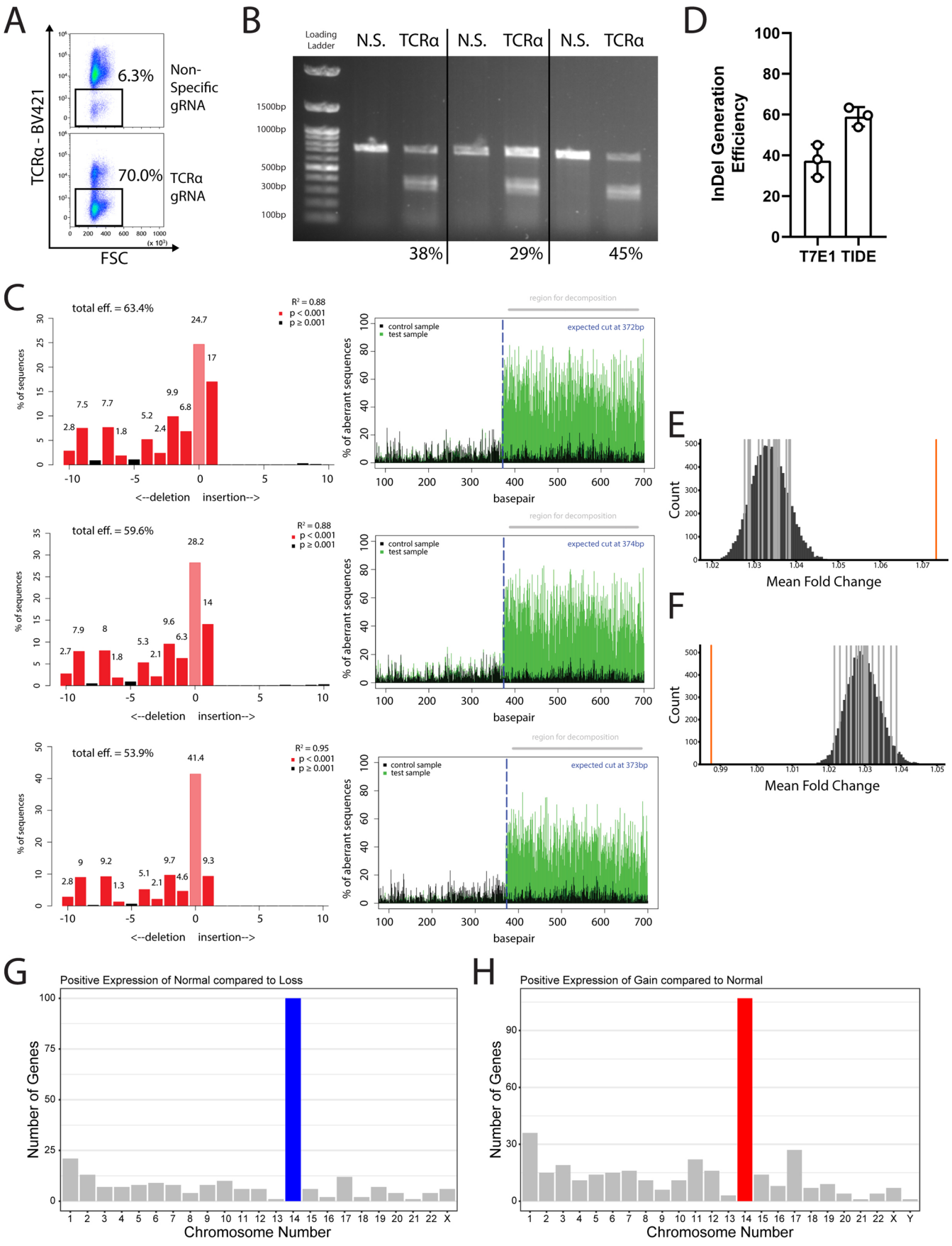

Extended Data Fig. 1 | See next page for caption.

Extended Data Fig. 1 | Quantification of InDels produced by CRISPR-Cas9 activity at the TCRα locus indicates efficient cleavage. A. Flow cytometry example of TCR ablation in primary human T cells following CRISPR-Cas9 RNP electroporation. Cells were electroporated with Cas9 and either a non-specific gRNA or a TCRα-targeting gRNA. **B**. T7 Endonuclease 1 (T7E1) assay for three independent experiments. For each experiment, one lane for non-Specific gRNA (N.S.) and one lane for TCRα-targeting gRNA treated cells are presented. Experiments are separated by a black bar. Percentages, presented below the lanes, refer to cleavage efficiency as inferred by densitometric analysis. Loading Ladder and relative sizes are indicated on the left. Unprocessed scan can be found in Supplementary Data 1. **C**. TIDE Analysis for the same experiments as in B. In the left panel, the height of each bar corresponds to the rate of sequences having the given number of nucleotides added or deleted. The right panel depicts the rate of sequence misalignments at each position of the PCR fragment amplified from the TCRα locus of cells treated with either the TCRα-targeting gRNA (green) or a non-Specific gRNA (black) **D**. Quantification of B and C. **E-F**. Enrichment in the number of genes with no detected expression among cells identified as having a chromosome 14 loss (E) or gain (F) in Fig. 1f. The x-axis represents the fold-change in the number of genes with no detected expression between cells with or without a chromosome 14 loss, based on the InferCNV analysis (Fig. 1f). The dark gray lines represent the empirical values obtained for each chromosome, except for chromosome 14. The orange line is the empirical value for chromosome 14. The black bars are the results of 10,000 permutations. **G**. Number of differentially expressed genes in each chromosome, as compared between cells with or without a chromosome 14 loss (see Fig. 1f). **H**. Number of differentially expressed genes in each chromosome, as compared between cells with or without a chromosome 14 gain (see Fig. 1f).

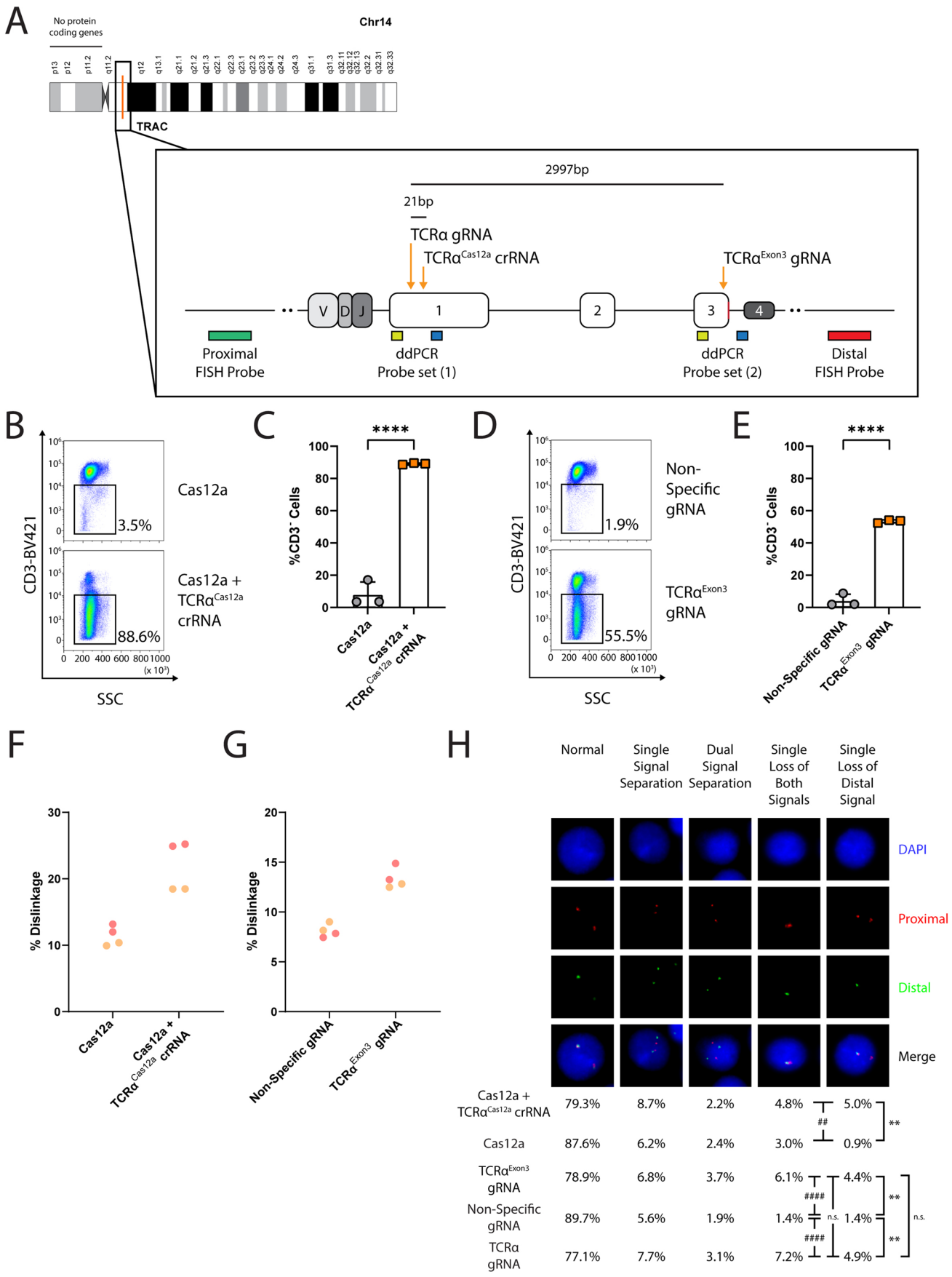

Extended Data Fig. 2 | See next page for caption.

Extended Data Fig. 2 | A. Schematic depiction of human chromosome 14 (Chr14). The target locus is indicated in orange. The zoomed in box indicates more specifically, the different target sites of each gRNA/crRNA used in this study. ddPCR and FISH probe sets are indicated below as colored yellow/blue or green/red boxes, respectively. Numbers above indicate distances, in base pairs (bp), between the targets. **B**. Flow cytometry example of TCR ablation in primary human T cells, 4 days following CRISPR-Cas12a RNP electroporation. Cells were electroporated with Cas12a alone or with Cas12a and the relevant crRNA. **C**. Quantification of B. Each dot represents an independent experiment. Mean value, standard deviation and individual experiments are indicated. n = 3, ****, $p < 0.0001$, two-sided unpaired Wilcoxon test. **D**. Flow cytometry example of TCR ablation in primary human T cells following CRISPR-Cas9 RNP electroporation. Cells were electroporated with Cas9 and either a non-specific gRNA or the TCRα-targeting gRNA in exon3 ($TCR\alpha^{exon3}$) as in A. **E**. Quantification of B. Each dot represents an independent experiment. Mean value, standard deviation and individual experiments are indicated. n = 3, ****, $p < 0.0001$, two-sided unpaired Wilcoxon test. **F-G** ddPCR dislinkage analysis 4 days following CRISPR-Cas12a electroporation (F) or CRISPR-Cas9 electroporation with the $TCR\alpha^{exon3}$ gRNA (G). Each color represents a different human donor. Each dot represents a technical replication. **H**. FISH analysis of cells treated with either Cas12a only, Cas12a + $TCR\alpha^{Cas12a}$ crRNA or Cas9 + a $TCR\alpha^{exon3}$-targeting gRNA. In the pictures are examples of all signal patterns found among analyzed cells. The frequency of each signal pattern among the electroporated cells is presented below the pictures. n = 338, n = 357 and n = 427 for cells electroporated with Cas12a only, Cas12a + $TCR\alpha^{Cas12a}$ crRNA or Cas9 + a $TCR\alpha^{exon3}$-targeting gRNA, respectively and n = 358 and n = 388 for cells electroporated with Cas9 + non-specific gRNA or Cas9 + TCRα targeting gRNA (as in Fig. 1a), respectively. **, $p = 0.0012$ for Fisher's exact test comparing loss of distal signal between cells transfected with Cas12a only and cells transfected with Cas12a + $TCR\alpha^{Cas12a}$ crRNA. ##, $p = 0.0015$ for Fisher's exact test comparing loss of either both signals or only the distal signal between cells transfected with Cas12a only and cells transfected with Cas12a + $TCR\alpha^{Cas12a}$ crRNA. ####, $p < 0.0001$ for Fisher's exact test comparing loss of distal signal between cells transfected with $TCR\alpha^{exon3}$ gRNA and cells transfected with a non-specific gRNA and for Fisher's exact test comparing loss of distal signal between cells transfected with TCRα gRNA and cells transfected with a non-specific gRNA. n.s., $p > 0.05$ for Fisher's exact test. comparing loss of distal signal between cells transfected with $TCR\alpha^{exon3}$ gRNA and cells transfected with TCRα gRNA. **, $p = 0.0069$ for Fisher's exact test comparing loss of only the distal signal between cells transfected with $TCR\alpha^{exon3}$ gRNA and cells transfected with a non-specific gRNA. **, $p = 0.0031$ for Fisher's exact test comparing loss of only the distal signal between cells transfected with the TCRα gRNA to cells transfected with a non-specific gRNA.

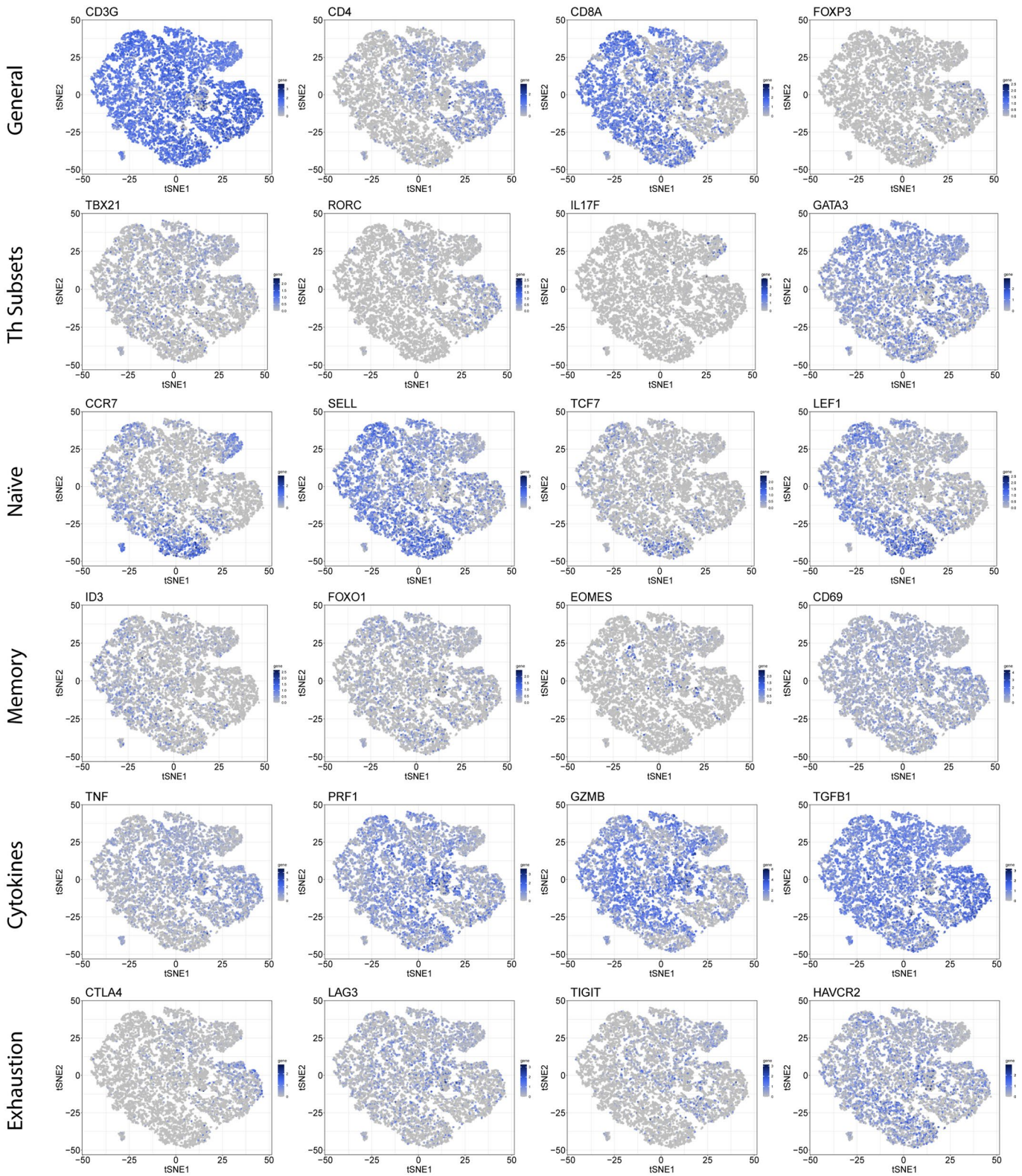

Extended Data Fig. 3 | Selected gene expression patterns across the cells. Each t-SNE plot represents all the cells in the experiment (Fig. 3a–c). Each plot represents the expression pattern of a different gene, indicated on the top left, among the clusters. A darker shade of blue corresponds to higher RNA expression. For each row, a title for the type of markers is indicated on the left.

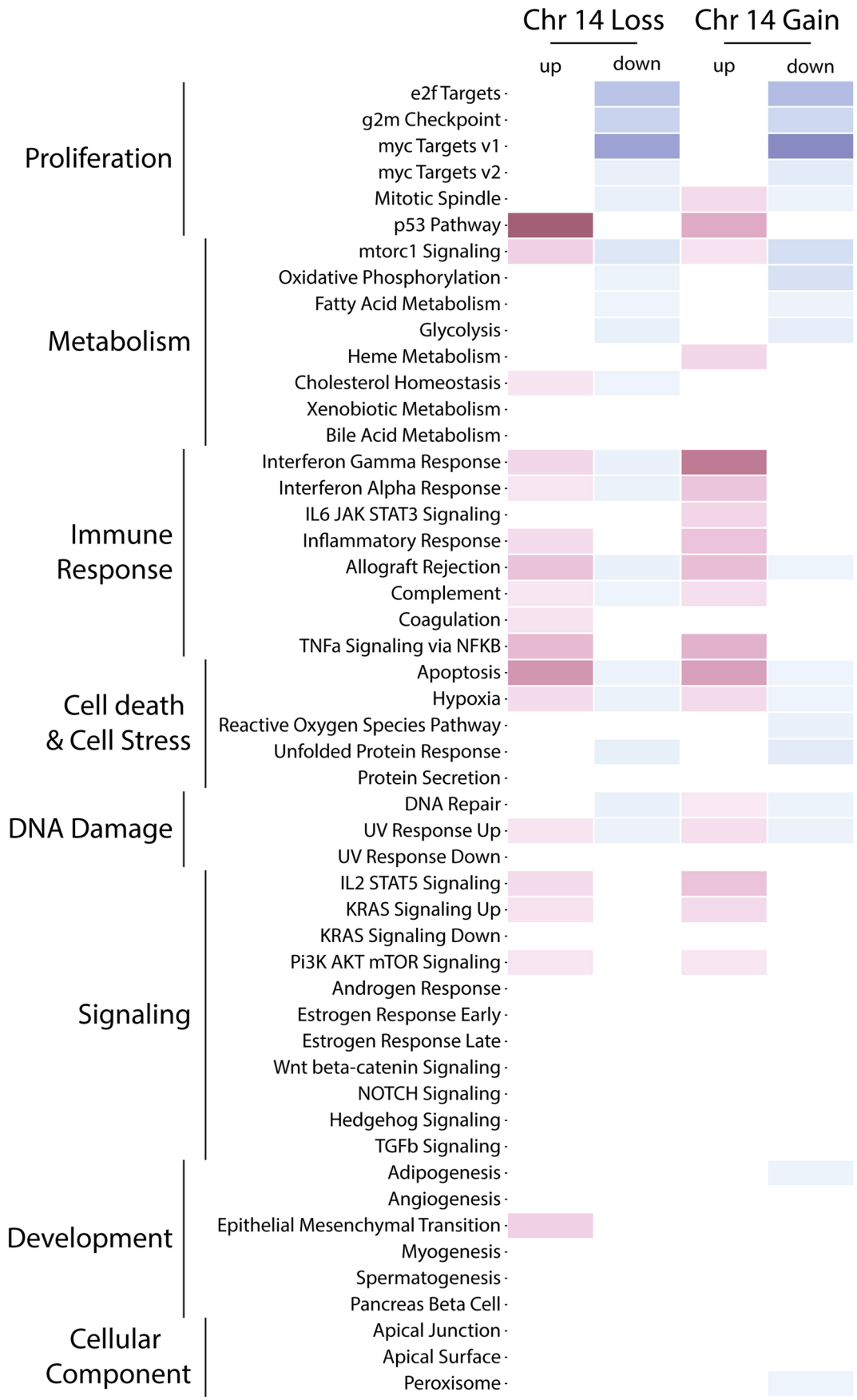

Extended Data Fig. 4 | See next page for caption.

Extended Data Fig. 4 | A gene set enrichment analysis between cells that have lost a copy of chromosome 14 (Fig. 1f), to cells without these chromosomal aberrations. The 50 'Hallmark' MSigDB gene sets are shown. Gene sets enriched in up-regulated genes are depicted in red and those enriched in down-regulated genes are depicted in blue. Values are scaled to -log(FDR) of the enrichments. The full enrichment scores are shown in Supplementary Table 1.

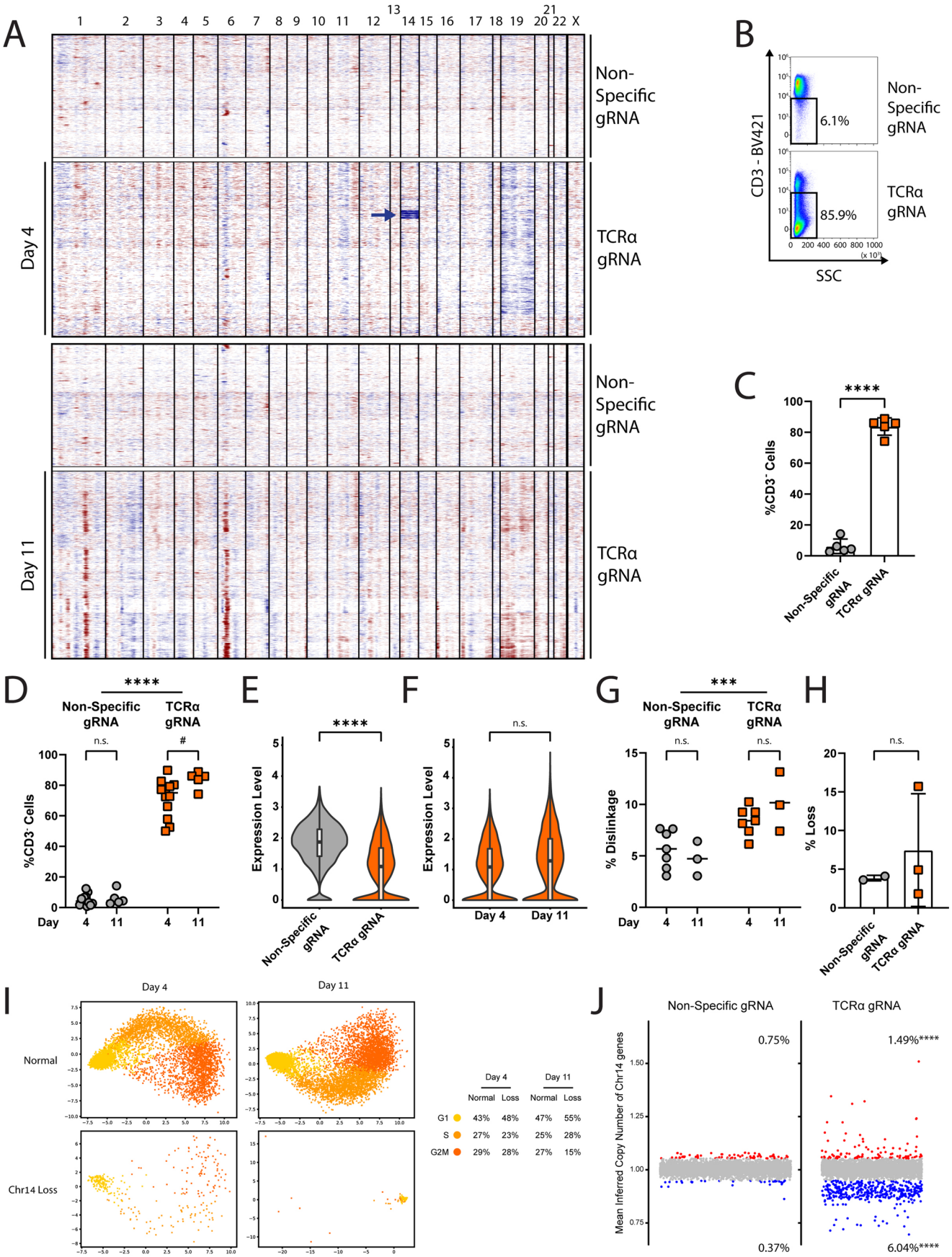

Extended Data Fig. 5 | See next page for caption.

Extended Data Fig. 5 | A. Heat map depicting gene copy numbers inferred from scRNAseq analysis following treatment with the TCRα-targeting gRNA 4 days (above) or 11 days (below) after CRISPR-Cas9 electroporation, as presented in Fig. 3h. The expression levels in cells treated with a non-specific gRNA 4 days after CRISPR-Cas9 electroporation served as a reference in both analyses. Each line represents an individual cell. The Chromosomes are ordered in columns and the color coding indicates an increase (red) or decrease (blue) in copy number of genes along the chromosomes (x-axis). **B**. Flow cytometry example of TCR ablation in primary human T cells, measured by CD3 staining, 11 days following CRISPR-Cas9 RNP electroporation. Cells were electroporated with Cas9 and either a non-specific gRNA or a TCRα-targeting gRNA. **C**. Quantification of B. Each dot represents an independent experiment. Mean value, standard deviation and individual experiments are indicated. n = 3, ****, $p < 0.0001$, two-sided unpaired t-test. **D**. CD3 expression from flow cytometry data at either 4 days or 11 days following CRISPR-Cas9 electroporation. n = 5-12, ****, $p < 0.0001$ for Two-Way ANOVA. #, $p = 0.0410$ and ns, $p > 0.05$ Tukey's multiple comparison. This plot includes data presented in Fig. 1c. **E**. A reduction in TCRα expression is evident in the scRNAseq, 4 days following CRISPR-Cas9 electroporation. The violin plots correspond to the TCRα expression level in cells treated with either a non-specific gRNA or the TCRα-targeting gRNA. Upper and lower boundaries as well as median and quartiles are indicated. ****, $p < 0.0001$, two-sided unpaired Wilcoxson test. **F**. A reduction of TCRα expression is stable in the scRNAseq, 11 days following CRISPR-Cas9 electroporation. The violin plots correspond to TCRα expression level in cells treated with the TCRα-targeting gRNA at either 4 days or 11 days following treatment. Upper and lower boundaries as well as median and quartiles are indicated. n.s., $p > 0.05$, two-sided unpaired Wilcoxson test. **G**. ddPCR dislinkage at either 4 days or 11 days following CRISPR-Cas9 electroporation. n = 3-7. Each dot represents the mean of replicates from an independent experiment, ***, $p = 0.0003$ and ns, $p > 0.05$ for Two-Way ANOVA and Tukey's multiple comparison, respectively. This plot includes the means of data presented in Fig. 2e. **H**. Quantification of FISH signals, from three independent experiments of T cells 11 days following CRISPR-Cas9 electroporation. Signal loss designates loss of either both signals or only the distal signal. Mean and Standard Deviations are indicated. n = 2-3, ns, non-significant two-sided unpaired t-test. **I**. Principal component (PC) analysis of cell cycle phase among cells treated with a TCRα-targeting gRNAs and characterized, as in Fig. 3h, as having a chromosome 14 loss (bottom) or not (normal, up) for cells 4 days following treatment (left) or 11 days following treatment (right). Legend and fraction of cells in each cell cycle phase is indicated on the right. **J**. Each dot represents the mean inferred copy number of genes coded on chromosome 14 in each cell treated with a non-specific gRNA (left) or a TCRα-targeting gRNA (right). Cells are marked with dots spread along the x-axis. The dots are colored red and blue when corresponding to cells with a chromosome 14 gain or loss respectively, at day 4 following treatment, if their mean inferred gene copy number is >2 standard deviations (blue and red), from the population's mean. ****, $p < 0.0001$ for Fisher's exact test comparing chromosome 14 gain or loss between cells treated with the TCRα gRNA and cells treated with a non-specific gRNA. Data with inferred gene copy number >3 standard deviations (blue and red), from the population's mean is presented in Fig. 3h.

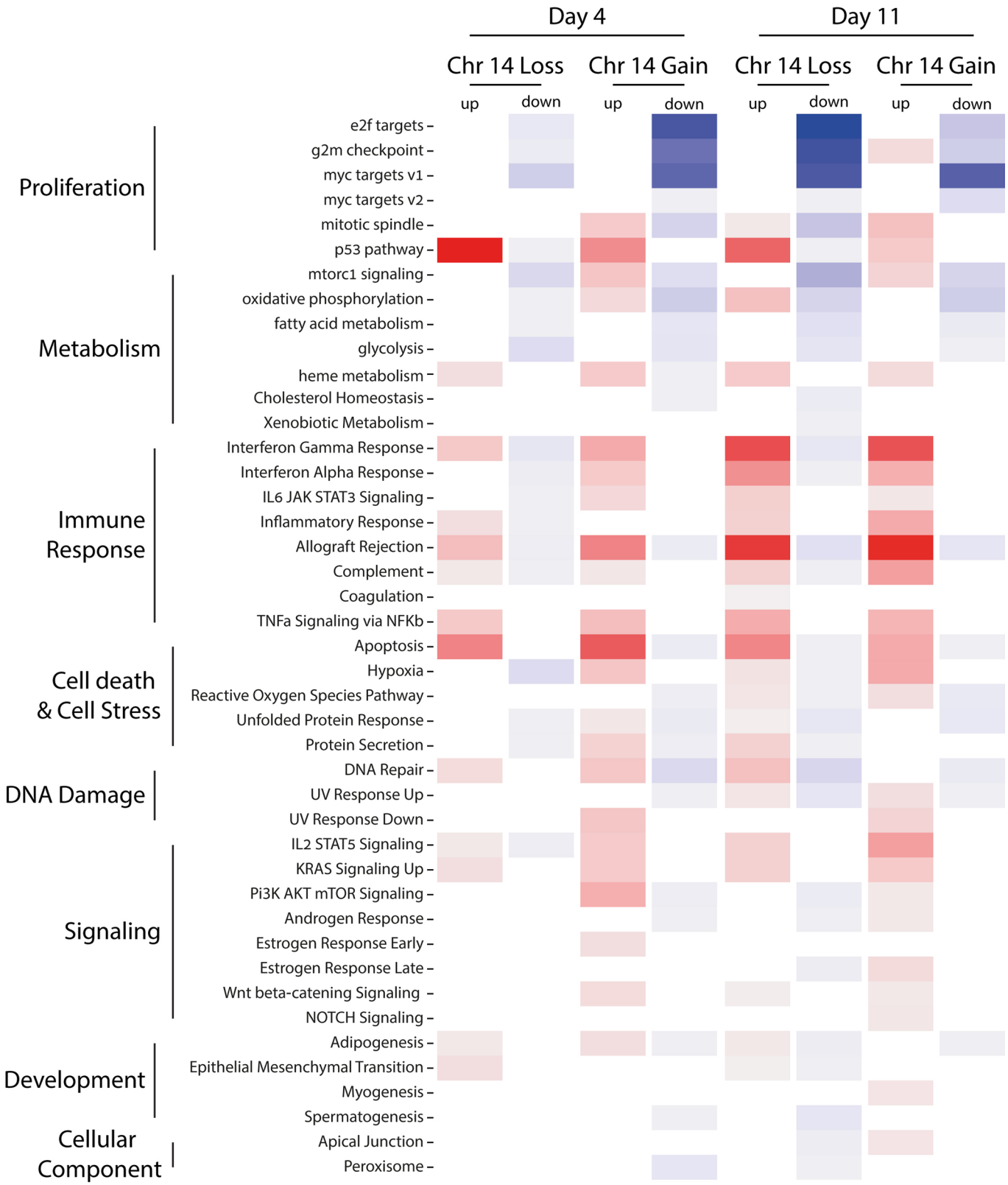

Extended Data Fig. 6 | A gene set enrichment analysis between cells that have lost or gained a copy of chromosome 14, 4 or 11 days following treatment, compared to cells without these chromosomal aberrations. The 50 'Hallmark' MSigDB gene sets are shown. Gene sets enriched in up-regulated genes are depicted in red and those enriched in down-regulated genes are depicted in blue. Values are scaled to -log(FDR) of the enrichments. The full enrichment scores are shown in Supplementary Table 1.

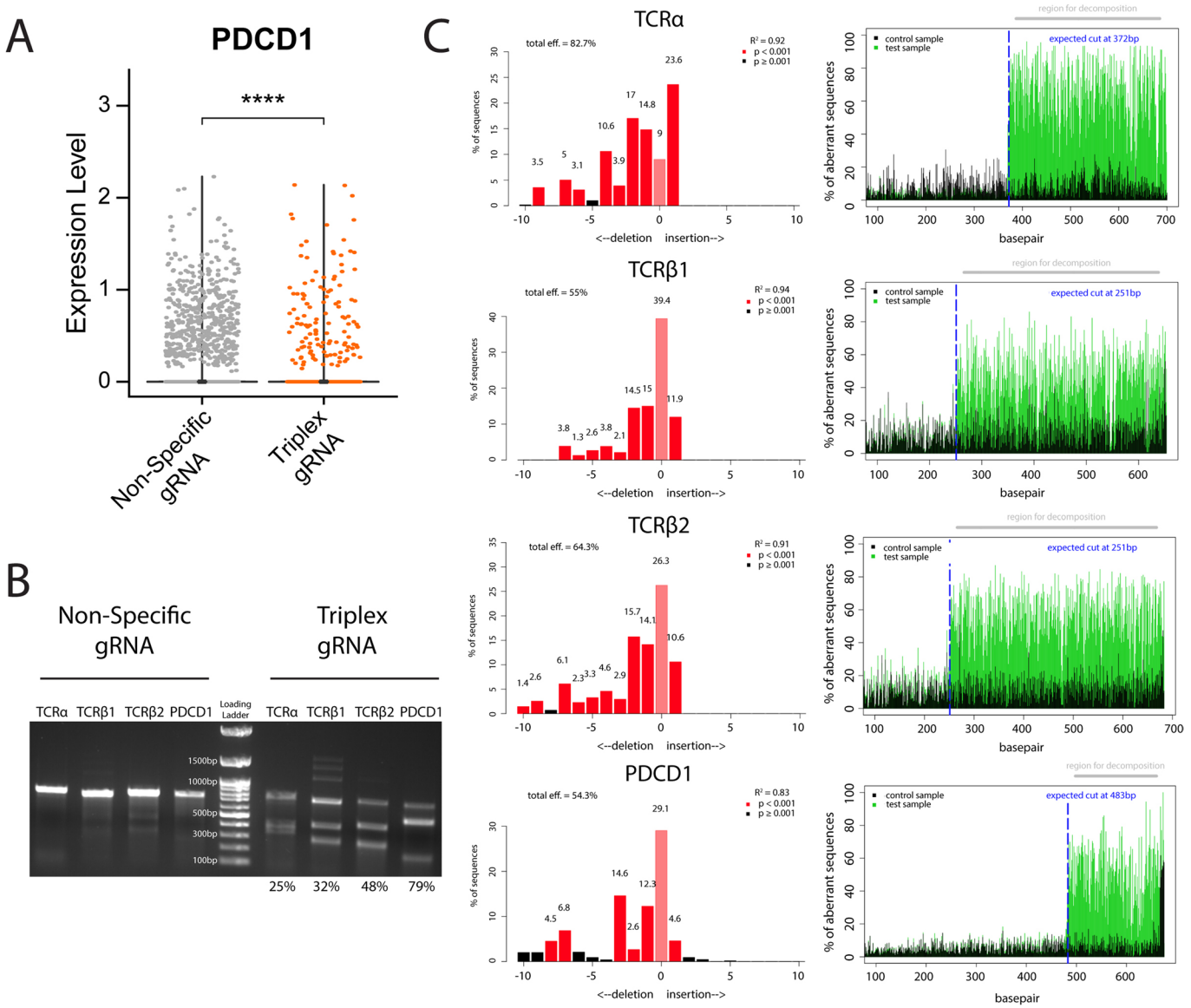

Extended Data Fig. 7 | Quantification of InDels produced by CRISPR-Cas9 activity at the TCRα, TCRβ and PDCD1 loci indicates efficient cleavage. **A**. RNA expression of PDCD1 in cells treated with either a non-specific gRNA or a combination of TCRα, TCRβs and PDCD1- targeting gRNAs. ****, $p < 0.0001$, two-sided unpaired Wilcoxon test. RNA expression presented as violin can be found in Fig. 4b. **B**. T7E1 assay for the 4 genomic target loci. Cells treated with a non-Specific gRNA (4 left lanes) are compared to cells treated with the combination of the TCRα, TCRβ and PDCD1- targeting gRNAs (4 right lanes). In each lane, a different locus is analyzed. Calculated efficiency is indicated below. Loading Ladder and relative sizes are indicated in the middle. Unprocessed scan can be found in Supplementary Data 1. **C**. TIDE Analysis for the same experiments as in A. The rows represent (in this order, from top to bottom) the TCRα, TCRβ1, TCRβ2 and PDCD1 loci. In the left panels, the height of each bar corresponds to the rate of sequences having the given number of nucleotides added or deleted. The right panels depict the rate of sequence misalignments at each position of the PCR fragment amplified from the target locus of cells treated with either a non-specific gRNA (black) or a combination of the TCRα, TCRβ and PDCD1- targeting gRNAs (green).

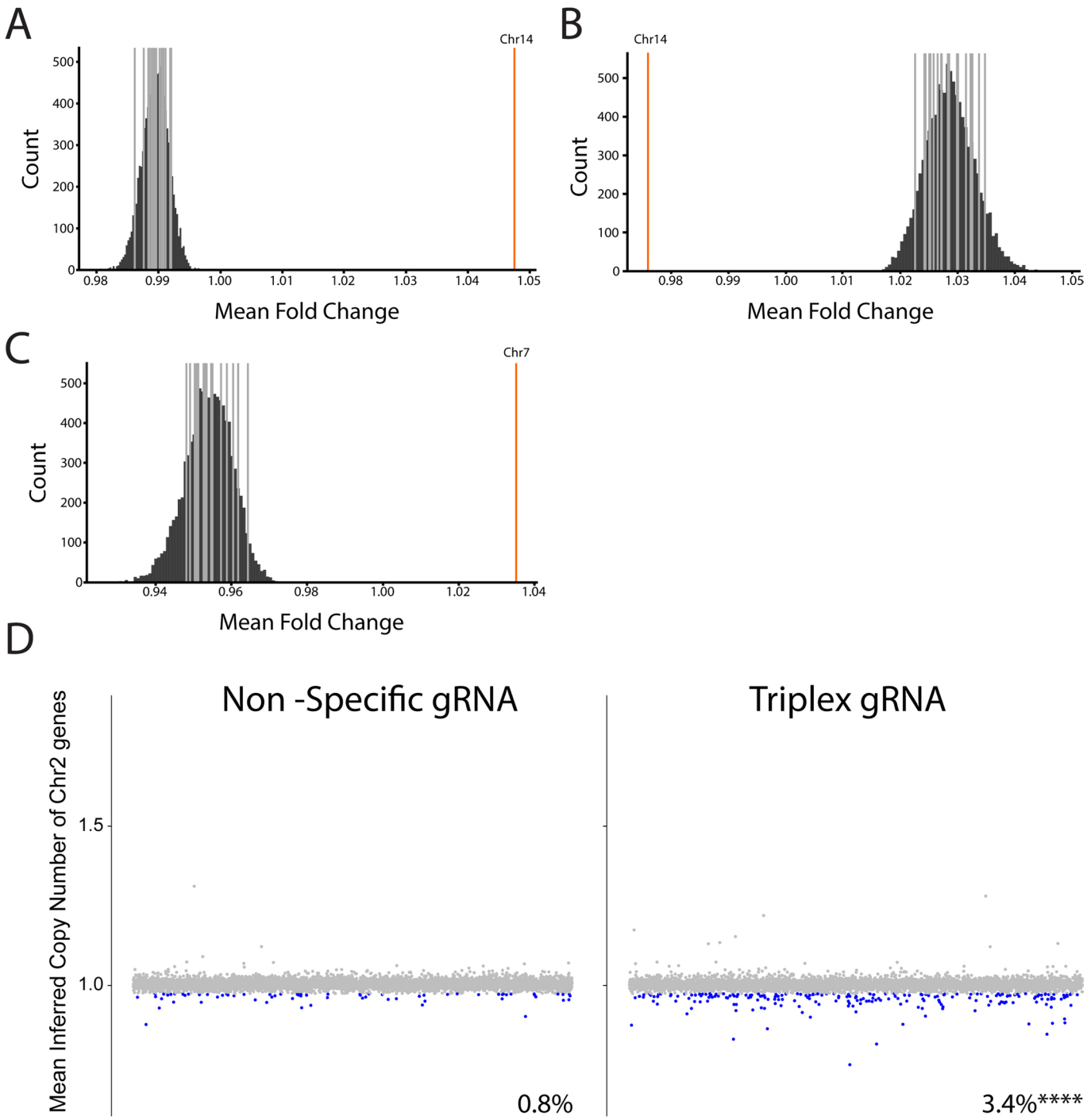

Extended Data Fig. 8 | Enrichment in the number of genes with no detected expression among cells identified as having a chromosome 14 loss (A), a chromosome 14 gain (B) or a chromosome 7 truncation (C) (Fig.4d). The x-axis represents the fold-change in the number of genes with no detected expression between cells with or without a chromosome 14 loss or gain or a chromosome 7 truncation, based on the InferCNV analysis (Fig. 4d). The dark gray lines represent the empirical values obtained for each chromosome, except for chromosome 14 or 7 in the respective plots. The orange line is the empirical value for chromosome 14 or chromosome 7. The black bars are the results of 10,000 permutations. **D**. Differential gene expression analysis for chromosome 2. Each dot represents the mean inferred copy number of genes coded on chromosome 2 in each cell treated with a non-specific gRNA (left) or a combination of the TCRα, TCRβ and PDCD1- targeting gRNAs (right). Cells are marked with dots spread along the x-axis. The dots are colored blue when corresponding to cells with a chromosome 2 loss, if their mean inferred gene copy number is >2 standard deviations from the population's mean. n = 8619 and 6326 for cells treated with a non-specific gRNA (left) or a combination of the TCRα, TCRβ and PDCD1- targeting gRNAs (right), respectively. ****, $p < 0.0001$ for Fisher's exact test comparing chromosome 2 loss between cells treated with the PDCD1 gRNA and cells treated with a non-specific gRNA.

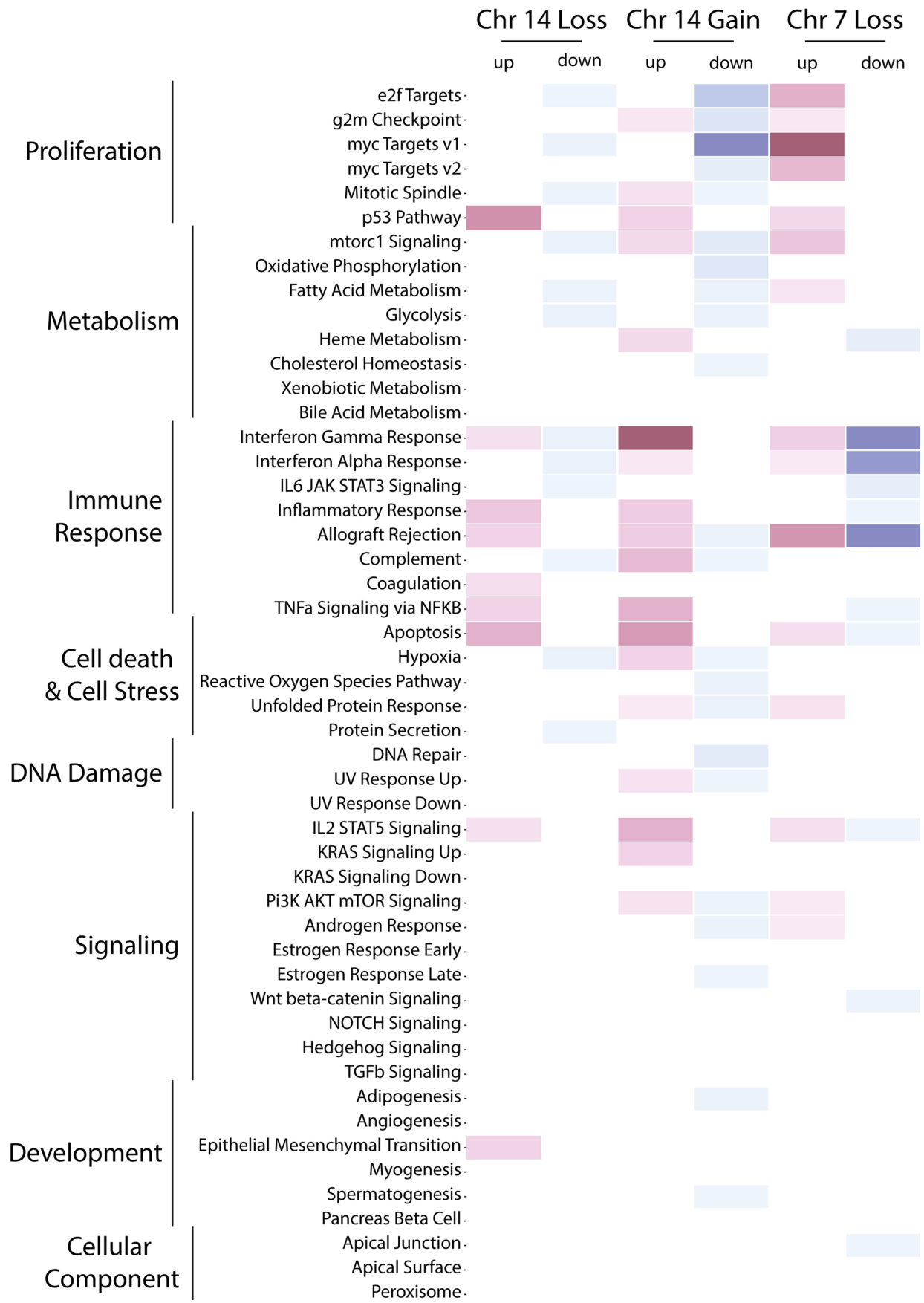

Extended Data Fig. 9 | See next page for caption.

Extended Data Fig. 9 | A gene set enrichment analysis between cells that have lost a copy of chromosome 14, or a segment of chromosome 7, to cells without these chromosomal aberrations. The 50 'Hallmark' MSigDB gene sets are shown. Gene sets enriched in up-regulated genes are depicted in red and those enriched in down-regulated genes are depicted in blue. Values are scaled to -log(FDR) of the enrichments. The full enrichment scores are shown in Supplementary Table 1.

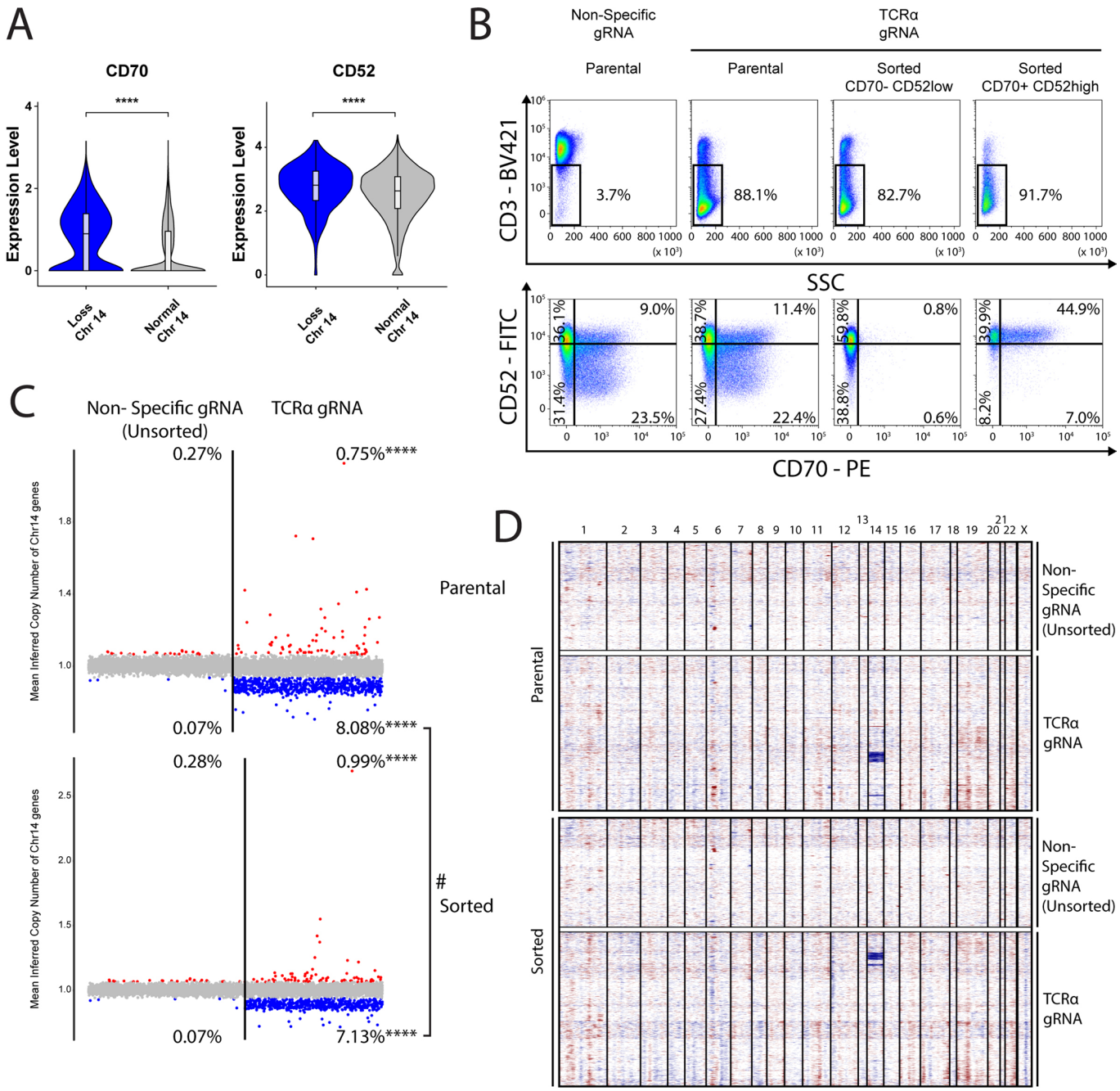

Extended Data Fig. 10 | Using the T cell surface markers CD70 and CD52 to sort out aberrant cells. A. The violin plots show gene expression of CD70 (left) and CD52(right), for cells treated with the combination of the TCRα, TCRβ and PDCD1- targeting gRNAs and having a normal gene expression (grey) or a gene expression pattern indicating a chromosome 14 loss(blue). **** $p < 0.0001$, unpaired two-tailed Wilcoxon test. **B**. Flow Cytometry of cells at day 4 following treatment with Cas9 and the TCRα targeting gRNA of cells sorted a day earlier for $CD70^{-}$ and $CD52^{low}$ or $CD70^{+}$ $CD52^{high}$. Plots marked as 'parental' include cells that went through the sorter, but were not sorted for a specific expression of the CD70 or CD52. **C**. Each dot represents the mean inferred copy number of genes coded on chromosome 14 in each cell treated with a non-specific gRNA (left) or the TCRα-targeting gRNA (right). InferCNV analysis performed 4 days following electroporation. Cells are marked with dots spread along the x-axis. The dots are colored red and blue when corresponding to cells with a chromosome 14 gain or loss respectively, if their mean inferred gene copy number is >2 standard deviations (blue and red), from the population's mean. n = 8642 and 8970 for 'parental' cells after treatment with a non-specific gRNA (left) or the TCRα-targeting gRNA(right), respectively. n = 8642 and 7598 for sorted cells after treatment with a non-specific gRNA (left) or TCRα-targeting gRNA (Right), respectively. The same dataset was used as a reference in both the InferCNV analyses (non-specific gRNA, Unsorted). ****, $p < 0.0001$ for Fisher's exact test comparing chromosome 14 gain or loss between cells treated with the TCRα gRNA and cells treated with a non-specific gRNA (unsorted). #, $p = 0.0257$ for Fisher's exact test comparing chromosome 14 loss between the parental cells treated with the TCRα gRNA and sorted cells treated with the TCRα gRNA. **D**. Heat map depicting gene copy numbers inferred from scRNAseq analysis following sorting of TCRα-targeted cells for either alive ('Parental', above) or $CD70^{-}$ $CD52^{low}$ expression (Sorted, below). Each line represents an individual cell. The Chromosomes are ordered in columns and the color coding indicates an increase (red) or decrease (blue) in copy number of genes along the chromosomes (x-axis). The same dataset was used as a reference in both the InferCNV analyses (non-specific gRNA, Unsorted).

nature portfolio

Corresponding author(s): Adi Barzel, Uri Ben-David & Asaf Madi

Last updated by author(s): May 18, 2022

Reporting Summary

Nature Portfolio wishes to improve the reproducibility of the work that we publish. This form provides structure for consistency and transparency in reporting. For further information on Nature Portfolio policies, see our Editorial Policies and the Editorial Policy Checklist.

Statistics

For all statistical analyses, confirm that the following items are present in the figure legend, table legend, main text, or Methods section.

n/a	Confirmed	
☐	☒	The exact sample size (*n*) for each experimental group/condition, given as a discrete number and unit of measurement
☐	☒	A statement on whether measurements were taken from distinct samples or whether the same sample was measured repeatedly
☐	☒	The statistical test(s) used AND whether they are one- or two-sided *Only common tests should be described solely by name; describe more complex techniques in the Methods section.*
☐	☒	A description of all covariates tested
☐	☒	A description of any assumptions or corrections, such as tests of normality and adjustment for multiple comparisons
☐	☒	A full description of the statistical parameters including central tendency (e.g. means) or other basic estimates (e.g. regression coefficient) AND variation (e.g. standard deviation) or associated estimates of uncertainty (e.g. confidence intervals)
☒	☐	For null hypothesis testing, the test statistic (e.g. *F*, *t*, *r*) with confidence intervals, effect sizes, degrees of freedom and *P* value noted *Give P values as exact values whenever suitable.*
☒	☐	For Bayesian analysis, information on the choice of priors and Markov chain Monte Carlo settings
☒	☐	For hierarchical and complex designs, identification of the appropriate level for tests and full reporting of outcomes
☒	☐	Estimates of effect sizes (e.g. Cohen's *d*, Pearson's *r*), indicating how they were calculated

Our web collection on statistics for biologists contains articles on many of the points above.

Software and code

Policy information about availability of computer code

Data collection	Data collection for flow cytometry was performed using Attune Nxt software
Data analysis	For single cell RNA sequencing, raw BCL files for the DNA sequencing data were processed using Cellranger DNA (version 5.0.1). Data were aligned to the 10X Genomics GRCh38 genome. Results were visualized in the Loupe scDNA Browser (version 5.0.0). Raw gene expression data were extracted from the Seurat object as recommended in the "Using 10x data" section (inferCNV of the Trinity CTAT Project, https://github.com/broadinstitute/inferCNV)

For manuscripts utilizing custom algorithms or software that are central to the research but not yet described in published literature, software must be made available to editors and reviewers. We strongly encourage code deposition in a community repository (e.g. GitHub). See the Nature Portfolio guidelines for submitting code & software for further information.

Data

Policy information about availability of data

All manuscripts must include a data availability statement. This statement should provide the following information, where applicable:

- Accession codes, unique identifiers, or web links for publicly available datasets
- A description of any restrictions on data availability
- For clinical datasets or third party data, please ensure that the statement adheres to our policy

All datasets are available within the article and its Supplementary Information. 10X scRNAseq data have been deposited to SRA with BioProject accession number PRJNA759387.

Field-specific reporting

Please select the one below that is the best fit for your research. If you are not sure, read the appropriate sections before making your selection.

☒ Life sciences ☐ Behavioural & social sciences ☐ Ecological, evolutionary & environmental sciences

For a reference copy of the document with all sections, see nature.com/documents/nr-reporting-summary-flat.pdf

Life sciences study design

All studies must disclose on these points even when the disclosure is negative.

Sample size	For flow cytometry, sample size for each condition was not predetermined. All replicates performed are presented in the text. For FISH, sample size for each experiment was not predetermined. For scRNAseq, for each experiment, sample size was calibrated for 17,000 cells were experiment, at a 1:1 ratio for non-specific gRNA treated cells and TRAC or TRAC, TRBC1-2 and PDCD1 treated cells.
Data exclusions	For InferCNV, the non-specific gRNA treated T cells were used as a reference and paramaters "denoise" default hidden markov model (HMM) settings and a value of 0.1 for "cutoff" were used.
Replication	Replication of the flow cytometry was performed independently, as indicated in the relevant figures in the manuscript. Replication for FISH was performed once on independent samples. The replicates are presented in the text and the supplementary materials. For scRNAseq, we performed two independent runs, as stated in the text. For the first, only TRAC was a targeted by CRISPR-Cas9. On the second run, TRAC TRBC1-2 and PDCD1 were targeted. Results for the TRAC were similar in both experiments, as stated in the text.
Randomization	Not relevant to the study. Each sample analyzed was divided into two groups: either treated with a non-relevant gRNA or with a gRNA targeting either TRAC or TRAC, TRBC1-2 and PDCD1.
Blinding	Investigators were not blinded during data collection and analysis.

Reporting for specific materials, systems and methods

We require information from authors about some types of materials, experimental systems and methods used in many studies. Here, indicate whether each material, system or method listed is relevant to your study. If you are not sure if a list item applies to your research, read the appropriate section before selecting a response.

Materials & experimental systems

n/a	Involved in the study
☐	☒ Antibodies
☒	☐ Eukaryotic cell lines
☒	☐ Palaeontology and archaeology
☒	☐ Animals and other organisms
☐	☒ Human research participants
☒	☐ Clinical data
☒	☐ Dual use research of concern

Methods

n/a	Involved in the study
☒	☐ ChIP-seq
☐	☒ Flow cytometry
☒	☐ MRI-based neuroimaging

Antibodies

Antibodies used	Brilliant violet 421 anti-human CD3 (Biolegend, clone OKT3, Cat: 317344, Lot: B264955, Dilution: 1/100) Brilliant violet 421 anti-human TCRa/b (Biolegend, clone IP26, Cat: 306722, Lot: B261746, Dilution: 1/100) PE anti-human CD70 (Biolegend, clone 113-16, Cat: 355104, Lot: B324455, Dilution: 1/100) FITC anti-human CD52 (Biolegend, clone HI186, Cat: 316004, Lot: B322707, Dilution: 1/100)
Validation	Each lot of these antibodies are tested by the manufacturer for immunofluorescent staining with flow cytometric analysis. anti-human CD3 clone IP26 has reported cross-reactivity with Chimpanzee anti-human CD52 clone HI186 has reported cross-reactivity with Cynomolgus and Rhesus

Human research participants

Policy information about studies involving human research participants

Population characteristics	Samples were obtained from random donors of the Israeli population
Recruitment	Blood was obtained from random consent donors from the Israeli Blood Bank (Magen David Adom, Sheiba Medical Center)

Ethics oversight	Tel Aviv University Review Board

Note that full information on the approval of the study protocol must also be provided in the manuscript.

Flow Cytometry

Plots

Confirm that:

☒ The axis labels state the marker and fluorochrome used (e.g. CD4-FITC).

☒ The axis scales are clearly visible. Include numbers along axes only for bottom left plot of group (a 'group' is an analysis of identical markers).

☒ All plots are contour plots with outliers or pseudocolor plots.

☒ A numerical value for number of cells or percentage (with statistics) is provided.

Methodology

Sample preparation	For Flow Cytometry cells were harvested, washed, and resuspended in Cell Staining Buffer (Biolegend) containing 1/100 diluted of the relevant antibody. Staining was performed for 15mins at room temperature in the dark. Finally, cells were washed before data acquisition. Cell sorting was performed 3 days following electroporation. Cells were harvested, washed and resuspended in PBS supplemented with 5% BSA containing 1/100 diluted anti-human CD70 and anti-human CD52 (Biolegend). Staining was performed for 15 mins at room temperature in the dark. Subsequently, cells were washed and resuspended in PBS supplemented with 0.5% BSA. During Fluorescence Activated Cell Sorting, cells were collected in MEM-Alpha (Biological Industries) supplemented with 0.5% Heat Inactivated FCS (Sigma) and P/S.
Instrument	Flow Cytometry experiments were performed on an Attune NxT Flow Cytometer (life Technologies). Sorting experiments were performed on BD FACSAria III (BD Biosciences)
Software	Flow cytometry data collection was performed on the Nxt Software v3.2.1 Data analysis was performed using Kaluza Analysis v2.1
Cell population abundance	Cell populations frequencies before and after sorting can be found in the relevant figures in the manuscript
Gating strategy	Cells were gated on singlets (according to SSC-A on SSC-H) and lymphocytes (according to FSC-A on SSC-A). Gating for specific markers can be found in the figures of the manuscript.

☐ Tick this box to confirm that a figure exemplifying the gating strategy is provided in the Supplementary Information.